Int. J. Solids Structures Vol. 28, No. 5, pp. 567–594, 1991
Printed in Great Britain.

0020–7683/91 $3.00 + .00
Pergamon Press plc

# STRESS VARIATION DUE TO AN IMPACT LINE LOAD ON A FOUR-PLY FIBRE COMPOSITE PLATE

W. A. GREEN
Department of Theoretical Mechanics, University of Nottingham, Nottingham NG7 2RD, U.K.

and

E. RHIAN GREEN
Department of Engineering, University of Leicester, Leicester LE1 7RH, U.K.

(*Received* 2 *April* 1990; *in revised form* 25 *October* 1990)

**Abstract**—The propagator matrix method together with the integral transform formalism is employed to derive the transient stress response in a fibre composite plate due to a normal impulsive line load acting on its upper surface. Each layer of the composite is modelled as a transversely isotropic elastic material which is inextensible along the fibre direction. The transform solutions are inverted numerically using data appropriate to a particular carbon fibre/epoxy resin composite. A discussion is given of the contributions from the individual modes associated with harmonic waves in the laminate, in terms of the variation of group velocity with wavenumber in the mode. Detailed plots are presented showing the stress variation with distance from the impact line at two different instants of time. These plots show the stress levels at the top and bottom suface of the plate, at the mid-surface and at the upper and lower interfaces between the plies.

## 1. INTRODUCTION

This paper extends our earlier results (Baylis and Green, 1988; Green and Baylis, 1988a,b) relating to stress wave transmission due to line impact loads acting on the surface of a four-ply laminate of fibre reinforced material. Each of the plies is modelled as a transversely isotropic elastic continuum with the axis of transverse isotropy lying in the plane of the ply and parallel to the fibre direction. This continuum approach means that we must restrict consideration to waves whose wavelengths are at least one order of magnitude greater than the fibre diameter and inter-fibre spacing so that on the scale of the wavelength the continuum theory might be expected to be valid. A typical material consists of a 60% volume fraction of carbon fibres embedded in a thermoplastic resin, for which the ply thickness, $h \simeq 125\ \mu$m, with the fibre diameter and inter-fibre spacing of the order of 6 $\mu$m. Thus we are thinking in terms of wavelengths of the order of 1/2 to 1/3 the ply thickness or greater, for which the non-dimensional wave number $kh = 2\pi h/\Lambda$ (where $\Lambda$ is the wavelength) varies from zero at infinite wavelength to a value of approximately 18 at $\Lambda = h/3$. For smaller wavelengths of the order of $h/10$ or less, the continuum model will break down due to diffraction and scattering by the individual fibres.

There is a considerable simplification in the mathematics to be gained by treating the composite as inextensible in the direction of transverse isotropy. This is an idealization of the fact that the extensional modulus of the continuum along the fibre direction can be of the order of 100 times that in the cross fibre direction. Mathematically, the effect of the idealization is to reduce the order of the differential equations and this leads to solutions involving fewer parameters. A consequence of this reduction in the order of the equations, however, is that it is no longer possible to satisfy all the interface continuity conditions between the plies. This leads to a singular perturbation problem, in which it is necessary to allow the tangential component of traction along the fibre direction to be discontinuous across the interface, with a consequent singularity in the stress component along the fibres, associated with a finite load carried by the surface layer of fibres. These stress discontinuities are to be interpreted in terms of very narrow bands (boundary layers) adjacent to the interfaces, through which there exist high stress gradients, giving large changes in stress across the bands. The associated singular stresses along the boundary fibres are to be

interpreted as high stress levels in the boundary layers, which contribute finite loads in the fibre directions when integrated through the boundary layers. It is with these interpretations in mind that we adopt the idealization of inextensibility to give a mathematically simple model of our fibre reinforced material. Detailed comparisons between the dynamic behaviour of the idealized inextensible model and of a continuum model which does not adopt the inextensibility constraint have been presented elsewhere (Green, 1982; Green and Milosavljević, 1985; Baylis and Green, 1986a,b), but a comparison of the results of the two models is included here for completeness.

In this paper we are concerned with a symmetric cross-ply configuration of the laminate in which the two inner layers are aligned with the fibre directions parallel to each other and at right angles to the fibre direction in the two outer layers. We make no assumptions about the variation of displacements and stresses through the laminate, such as is done in engineering theories of plates and shells. Our method is to solve exactly the system of governing equations appropriate to each layer, matching the solutions across the interfaces and satisfying the appropriate boundary conditions at the upper and lower surfaces of the laminate. The method of solution involves taking Laplace transforms in time and Fourier transforms in the in-plane spatial coordinates of the governing equations of the model, and yields the exact solution for the variation of the transforms with depth throughout the laminate. The approximations arise only in the numerical methods for inverting the transforms.

The results presented in Baylis and Green (1988) relate to a line impact load oriented at an angle of 60° to the fibre direction in the outer layers. This generates a plane wave disturbance travelling in the plane of the laminate along the normal to the line load. Most of the results displayed in that paper show the variation of normal displacement at the upper and lower surfaces of the plate as a function of distance along the direction of travel, at various time after impact. The same paper also reports details of the tangential surface displacement variation with distance and of the surface stress variation with distance at both the upper and lower surfaces of the plate at one fixed time. More detailed results are presented in Green and Baylis (1988b) which deals with line loads oriented at 0°, 30°, 45°, 60° and 90° to the fibre direction in the outer layer. In addition to displaying the normal displacement on the upper and lower surfaces of the laminate, graphs are also presented showing the variation of the displacement normal to the plate as a function of distance from the impact line, at the interfaces between each of the plies at fixed times. These results bring out the existence of a Rayleigh surface wave disturbance at some orientations of the impact load and its absence at others.

Here we are concerned with a study of the stresses resulting from the line load impact on the upper surface of the four-ply plate. Attention is restricted to impacts oriented at 30° and 60° to the outer fibre direction since these two situations suffice to show the different nature of the responses. The transient stresses are evaluated at the outer surfaces of the plate, at the mid-plane and at the interfaces between the plies. We display our results as sets of curves showing the variations of stress along the normal to the impact line in the direction of travel as a function of distance from the impact line. These results relate to two instants of time. The first of these corresponds to the time taken for the fastest body wave in the medium to travel a distance of 10 times the overall plate thickness. The second is the time taken for the same wave to travel a distance of 50 times the plate thickness. The sets of curves display three different components of stress. Two of these are the two orthogonal shear tractions which act on each interface and on the upper and lower surfaces, the directions of the stresses being parallel to the two (orthogonal) fibre directions. The third stress component is the in-plane normal stress acting along the fibre direction of the outer layers and this also is evaluated at the upper and lower surfaces and at the interfaces. Our earlier work has drawn attention to the existence of a Rayleigh surface type wave travelling along the top surface for one range of impact angles and its non-existence outside this range. The curves shown here confirm this phenomenon and demonstrate its decay with depth into the laminate. In addition, they furnish comparisons of the magnitudes of the stress components associated with different angles of propagation and the variation of stress level with depth in the laminates.

The object of this theoretical investigation is to determine the nature of the three-dimensional stress wave transmission in a fibre composite laminate under the assumption of complete bonding between the plies. Such a situation can serve a two-fold purpose. In the first place, as pointed out by Mal (1988), it can provide a standard against which to compare the results of non-destructive evaluation (NDE) measurements aimed at locating flaws in the laminate. Secondly, it provides information on the channelling of disturbances within individual layers and along particular orientations relative to the fibres (see for example Kreis and Sayir, 1983) and this serves to indicate regions at which impact stress levels may be higher than would be anticipated from predictions based on simple plate theories.

The solution techniques developed in our earlier papers allow us to evaluate displacements and stresses throughout the laminate and it is a report on the stresses which will be our main concern here. In Section 2 we review the solution technique and obtain detailed expressions for the displacement and stress transforms at the middle surface and the two interfaces of the four-ply plate. Section 3 contains a brief account of the numerical inversion of the transforms whilst the detailed solutions are presented and discussed in Section 4.

Transient problems in elastic waveguides have been extensively studied by Miklowitz and his co-workers and a comprehensive account of the early work is to be found in the monograph by Miklowitz (1978). Among the more recent studies which have a relevance to the present work we cite the papers of Ceranoglu and Pao (1981), Weaver and Pao (1982) and Vasudevan and Mal (1985), which treat isotropic plates, and the paper by Willis and Bedding (1978), which is concerned with anisotropic plates and layers. These studies all approach the problem using the full three-dimensional equations of motion. An alternative technique is to make use of an engineering type plate theory which makes some simplifying assumption about the nature of the variation of stress through the laminate, and results in equations of motion involving only the in-plane space variables. An example of this technique is to be found in the paper by Chow (1971), who deals with the impact response of a simply supported laminated plate. This is also the approach adopted in the papers by Moon (1972) and Sun (1973), who plot the wave fronts due to a point impact on symmetric and asymmetric angle-ply laminates, respectively. A third alternative method is exemplified in the papers by Lee *et al.* (1984) and by Wu and Springer (1988), which both employ the finite element numerical technique to evaluate the transient stresses induced by impact on composite plates.

## 2. GOVERNING EQUATIONS AND TRANSFORM SOLUTIONS

We choose a Cartesian coordinate system of axes with the origin in the mid-plane of the plate, the $x_1$-axis normal to the plane of the layers, the $x_2$-axis parallel to the fibre directions in the two outer layers of the plate and the $x_3$-axis parallel to the fibre directions in the two inner layers of the plate as depicted in Fig. 1. Despite the fact that the layers are all of the same materials, we find it useful to designate the layers with the fibre direction parallel to $x_3$ as material 1 and the layers with fibre directions parallel to $x_2$ as material 2 and denote stress and displacement components in the layers with the corresponding suffix. The line load which produces the disturbance is taken to be a delta function in time and it is assumed to act on the upper surface of the plate, along a line making an angle $(\pi/2-\gamma)$ with the $x_3$-axis giving rise to waves travelling in the plane at an angle $-\gamma$ with the $x_3$-axis (see Fig. 1). The displacement components $u_i(x_1, x_2, x_3, t)$, $(i = 1, 2, 3)$, and the stress components $t_{ij}(x_1, x_2, x_3, t)$, $(i, j = 1, 2, 3)$ at time $t$ in each layer of the laminate then become functions $u_i(x_1, x, t)$ and $t_{ij}(x_1, x, t)$ of $x_1, t$ and $x = x_2 \sin\gamma + x_3 \cos\gamma$, only. The stress components are related to the displacement components through the stress–strain relations appropriate to each layer and these relations are given in detail by Baylis and Green (1986a). The stress components and displacement components must satisfy the equations of motion in each layer, together with continuity conditions at the interfaces between layers, traction-free conditions on the bottom surface of the plate and the specified loading conditions on the upper surface.

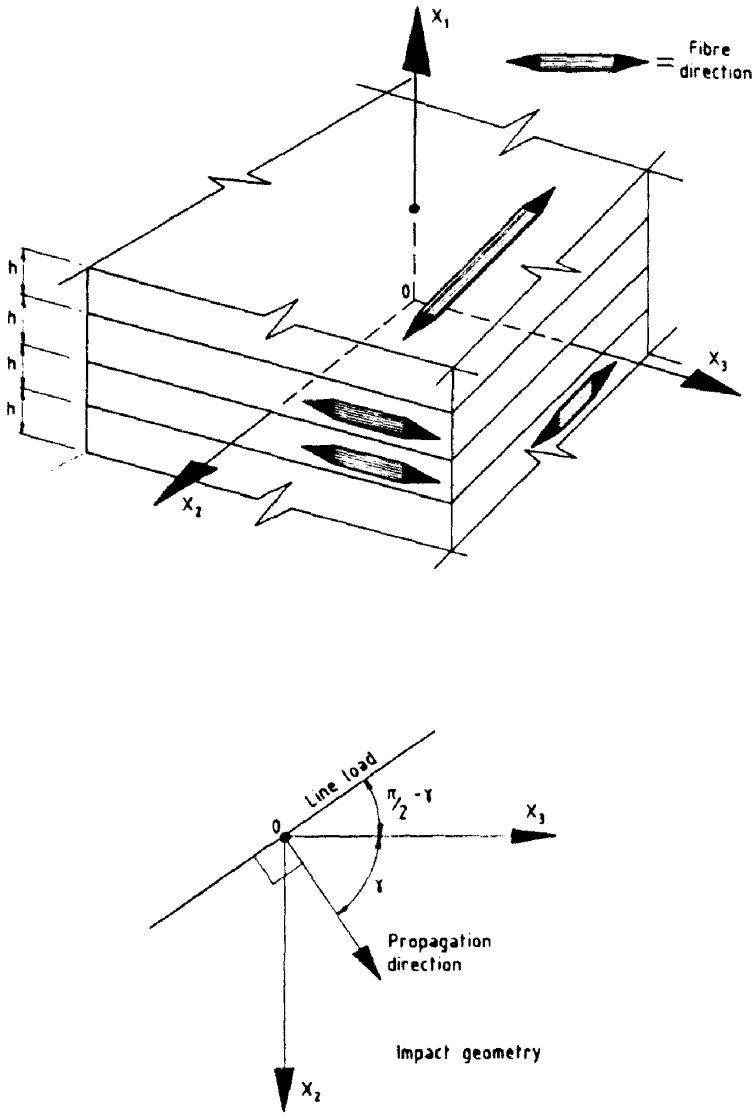


Fig. 1. Geometry of the laminate and the impact loading.

In order to solve the problem, it is convenient to work with the quantities $U$, $V$, $W$, $T_{ij}$, which are obtained from the displacement components $u_1$, $u_2$, $u_3$ and the stress components $t_{ij}$ respectively by taking Laplace transforms with respect to time $t$ and Fourier transforms with respect to the variable $x$. These are typified by the equation

$$U(x_1, k, s) = \int_{-\infty}^{\infty} \int_0^{\infty} u_1(x_1, x, t)\, e^{-st} e^{-ikx}\, dt\, dx. \tag{1}$$

Thus, $U$, $V$, $W$, and $T_{ij}$ are functions of the coordinate $x_1$ normal to the plane of the plate only, but they also involve the Laplace transform parameter $s$ and the Fourier transform parameter $k$. The equations of motion and stress-strain relations in each layer then reduce to a system of ordinary differential equations and algebraic relations to determine the transformed displacements and stresses within the layer as functions of $x_1$. The interface continuity conditions become a system of algebraic equations relating the transformed quantities between one layer and the next. Because of the inextensibility constraints the displacement transform $W$ is identically zero in material 1 and the transform $V$ is identically

zero in material 2. The governing equations in material 1 then have the form

$$\frac{dU_1}{dx_1} = \frac{c_2^2}{c_1^2} T_1 - \left(1 - \frac{2c_2^2}{c_1^2}\right) iksV_1,$$

$$\frac{dV_1}{dx_1} = P_1 - iksU_1,$$

$$\frac{dT_1}{dx_1} = \frac{(\hat{s}^2 + k^2c^2c_3^2)}{c_2^2} U_1 - iksP_1,$$

$$\frac{dS_1}{dx_1} = \left[4k^2s^2\left(1 - \frac{c_2^2}{c_1^2}\right) + \frac{k^2c^2c_3^2 + \hat{s}^2}{c_1^2}\right] V_1 - iks\left(1 - \frac{2c_2^2}{c_1^2}\right) T_1, \tag{2}$$

where

$$T_1 = \frac{T_{11}}{\rho c_2^2}, \quad P_1 = \frac{T_{12}}{\rho c_2^2}, \quad c = \cos\gamma \quad \text{and} \quad s = \sin\gamma.$$

In these expressions, $c_1$, $c_2$, $c_3$ are body wave speeds defined in terms of the elastic constants of the continuum material (see Green, 1982) and $\rho$ is the material density. Equations (2) have the solution

$$\mathbf{Y}(x_1) = \mathbf{P}(x_1 - \bar{x}_1)\mathbf{Y}(\bar{x}_1) \tag{3}$$

where

$$\mathbf{Y}(x_1) = (T_1(x_1)P_1(x_1)U_1(x_1)V_1(x_1))^{\mathrm{T}}$$

and T denotes the transpose. Equations (3) relate the value of the vector Y at any level $x_1$ in the layer to its value at some specified level $\bar{x}_1$ through the propagator matrix $\mathbf{P}(x_1 - \bar{x}_1)$. The elements $p_{ij}$ of the matrix $\mathbf{P}(h)$ corresponding to $x_1 - \bar{x}_1 = h$ are given in Table 1.

The parameters $p_1$, $p_2$ and $\alpha$ are defined in terms of the phase velocity $v = -i\hat{s}/k = \omega/k$ by the relations

$$c_1^2p_1^2 = c_1^2s^2 + c_3^2c^2 - v^2, \quad c_2^2p_2^2 = c_2^2s^2 + c_3^2c^2 - v^2, \quad \alpha = 1 - \frac{2c_2^2s^2}{(v^2 - c_3^2c^2)},$$

and $S_1$, $C_1$, $S_2$, $C_2$ are defined as

$$S_1 = \sinh p_1kh, \quad C_1 = \cosh p_1kh, \quad S_2 = \sinh p_2kh, \quad C_2 = \cosh p_2kh.$$

All the stress transforms $T_{ij}(x_1)$ which do not appear in Y are expressible in terms of the

Table 1. Elements of the propagator matrix $\mathbf{P}(h)$

| | | | |
|---|---|---|---|
| $\alpha C_1 + (1-\alpha)C_2$ | $\frac{i\alpha sS_1}{p_1} + (1-\alpha)\frac{ip_2S_2}{s}$ | $-\frac{2\alpha^2s^2kS_1}{(1-\alpha)p_1} + (1-\alpha)2p_2kS_2$ | $2i\alpha sk(C_1 - C_2)$ |
| $-(1-\alpha)\frac{ip_1S_1}{s} - \frac{i\alpha sS_2}{p_2}$ | $(1-\alpha)C_1 + \alpha C_2$ | $2i\alpha sk(C_1 - C_2)$ | $2(1-\alpha)kp_1S_1 - \frac{2k\alpha^2s^2S_2}{(1-\alpha)p_2}$ |
| $-\frac{(1-\alpha)}{2k}\left(\frac{p_1S_1}{s^2} - \frac{S_2}{p_2}\right)$ | $-\frac{(1-\alpha)i}{2sk}(C_1 - C_2)$ | $\alpha C_1 + (1-\alpha)C_2$ | $-(1-\alpha)\frac{ip_1S_1}{s} - \frac{i\alpha sS_2}{p_2}$ |
| $-\frac{(1-\alpha)}{2sk}i(C_1 - C_2)$ | $\frac{(1-\alpha)}{2k}\left(\frac{S_1}{p_1} - \frac{p_2S_2}{s^2}\right)$ | $\frac{i\alpha sS_1}{p_1} + (1-\alpha)\frac{ip_2S_2}{s}$ | $(1-\alpha)C_1 + \alpha C_2$ |

components of $\mathbf{Y}(x_1)$ and are given by the relations

$$T_{22} = \rho(c_1^2 - 2c_2^2)\frac{c_2^2}{c_1^2}T_1 + iks\rho 4c_2^2\left(1 - \frac{c_2^2}{c_1^2}\right)V_1,$$

$$T_{23} = \rho c_2^2 ikcV_1, \quad T_{31} = \rho c_2^2 ikcU_1,$$

$$T_{33} = -\rho\frac{c_2^2 c_2^2}{c_1^2}(T_1 + 2iksV_1). \tag{4}$$

In material 2 the governing equations may be written as a system of four first order equations similar to eqns (2) but involving $T_2$, $U_2$, $W_2$ and $R_2 = T_{13}/\rho c_2^2$ as dependent variables. Introducing the vector

$$\mathbf{Z} = (T_2(x_1)R_2(x_1)U_2(x_1)W_2(x_1))^{\mathrm{T}}$$

the solution of these equations has the form

$$\mathbf{Z}(x_1) = \mathbf{Q}(x_1 - \tilde{x}_1)\mathbf{Z}(\tilde{x}_1), \tag{5}$$

where $\tilde{x}_1$ is some specified level in the layer of material 2, $x_1$ is any other level in the same layer and $\mathbf{Q}(x_1 - \tilde{x}_1)$ is the propagator matrix for material 2. The elements of $q_{ij}$ of $\mathbf{Q}(h)$ may be obtained from those of $\mathbf{P}(h)$ by making the substitutions indicated in Table 2.

The quantities appearing in Table 2 are defined by the expressions

$$c_1^2 q_1^2 = c_1^2 c^2 + c_1^2 s^2 - v^2, \quad c_2^2 q_2^2 = c_2^2 c^2 + c_1^2 s^2 - v^2, \quad \hat{\alpha} = 1 - \frac{2c_2^2 c^2}{(v^2 - c_1^2 s^2)}$$

$$\hat{S}_1 = \sinh q_1 kh, \quad \hat{C}_1 = \cosh q_1 kh, \quad \hat{S}_2 = \sinh q_2 kh, \quad \hat{C}_2 = \cosh q_2 kh.$$

The remaining stress transforms at the level $x_1$ in this layer may be expressed in terms of the components of $\mathbf{Z}(x_1)$ through the equations

$$T_{22} = -\rho\frac{c_2^2 c_2^2}{c_1^2}(T_2 + 2ikcW_2),$$

$$T_{23} = \rho c_2^2 iksW_2, \quad T_{12} = \rho c_2^2 iksU_2,$$

$$T_{33} = \rho\frac{c_2^2}{c_1^2}(c_1^2 - 2c_2^2)T_2 + 4\rho c_2^2 ikc\left(1 - \frac{c_2^2}{c_1^2}\right)W_2. \tag{6}$$

The interface conditions at the mid-plane of the plate between the two layers of material 1 require the continuity of all three components of the displacement transforms and the continuity of the transformed stress components $T_{11}(= \rho c_2^2 T_1)$, $T_{12}(= \rho c_2^2 P_1)$ and $T_{13}$. Since the displacement transform $W_1$ is zero in both layers and the stress transform $T_{13}$ is given in terms of $U_1$ by eqns (4), these conditions are satisfied by the continuity of $\mathbf{Y}$ across the interface. At the interfaces $x_1 = -h$ and $x_1 = h$ between materials 1 and 2, we again require continuity of the three components of the displacement transforms but for the transformed stresses it is only necessary to ensure continuity of the normal component $T_{11}$. This is because the inextensibility constraint $W_1 = 0$ in material 1 allows the possibility of

Table 2. Transformation taking elements $p_{ij}$ into $q_{ij}$

| | | | |
|---|---|---|---|
| $p_1 \to q_1$, | $p_2 \to q_2$, | $\alpha \to \hat{\alpha}$, | $s \leftrightarrow c$ |
| $S_1 \to \hat{S}_1$, | $C_1 \to \hat{C}_1$, | $S_2 \to \hat{S}_2$, | $C_2 \to \hat{C}_2$ |

a discontinuity in the transformed component of traction $T_{13}$ across the interface (with an associated singularity in $T_{33}$) whilst the inextensibility constraint $V_2 = 0$ in material 2 allows a discontinuity in $T_{12}$ across the interface (with an associated singularity in $T_{22}$). We apply these conditions in two stages choosing first to satisfy the requirement that $V_1 = 0$ at $x_1 = \pm h$ where material 1 is bonded to material 2. Using the solution (3) with $\bar{x}_1 = 0$ and choosing $x_1 = h$ and $x_1 = -h$ gives

$$\mathbf{Y}(h) = \mathbf{P}(h)\mathbf{Y}(0), \quad \mathbf{Y}(-h) = \mathbf{P}(-h)\mathbf{Y}(0) \tag{7}$$

and the conditions $V_1(h) = 0$, $V_1(-h) = 0$ yield the equations

$$\begin{aligned} p_{41}T_1(0) + p_{42}P_1(0) + p_{43}U_1(0) + p_{44}V_1(0) &= 0, \\ P_{41}T_1(0) - p_{42}P_1(0) - p_{43}U_1(0) + p_{44}V_1(0) &= 0. \end{aligned} \tag{8}$$

In eqns (8) $p_{ij} = p_{ij}(h)$ and we have used the fact that $p_{41}$ and $p_{44}$ are even functions of $h$ whilst $p_{42}$ and $p_{43}$ are odd functions of $h$. Equations (8) may be solved to give $P_1(0)$ in terms of $U_1(0)$ and to give $V_1(0)$ in terms of $T_1(0)$ so that the vector $\mathbf{Y}(x_1)$ at any point in the core may be expressed in terms of the vector $\mathbf{X}_1(0) = (T_1(0)U_1(0))^{\mathrm{T}}$ only. In particular we may use the solutions of eqns (8) in eqns (7) to determine the vectors $\mathbf{X}_1(h)$ and $\mathbf{X}_1(-h)$ at the upper and lower interfaces in the form

$$\mathbf{X}_1(h) = \mathbf{R}\mathbf{X}_1(0), \quad \mathbf{X}_1(-h) = \tilde{\mathbf{R}}\mathbf{X}_1(0), \tag{9}$$

where the components of the $2 \times 2$ matrix $\mathbf{R}$ are given by

$$\begin{aligned} r_{11} &= p_{11} - \frac{p_{14}p_{41}}{p_{44}}, \quad r_{12} = p_{13} - \frac{p_{12}p_{43}}{p_{42}}, \\ r_{21} &= p_{31} - \frac{p_{34}p_{41}}{p_{44}}, \quad r_{22} = p_{33} - \frac{p_{32}p_{43}}{p_{42}} \end{aligned} \tag{10}$$

and

$$\tilde{\mathbf{R}} = \begin{pmatrix} r_{11} & -r_{12} \\ -r_{21} & r_{22} \end{pmatrix}. \tag{11}$$

The second of eqns (9) may be inverted and combined with the first to give the relation between $\mathbf{X}_1(h)$ and $\mathbf{X}_1(-h)$ as

$$\mathbf{X}_1(h) = \frac{\mathbf{R}\hat{\mathbf{R}}}{\det|\mathbf{R}|}\mathbf{X}_1(-h), \tag{12}$$

where

$$\hat{\mathbf{R}} = \begin{pmatrix} r_{22} & r_{12} \\ r_{21} & r_{11} \end{pmatrix}. \tag{13}$$

In the upper layer of the plate, which consists of material 2, we use eqn (5) with $\bar{x}_1 = h$ and $x_1 = 2h$ to relate the vector $\mathbf{Z}(2h)$ at the top of the layer to $\mathbf{Z}(h)$ at the bottom. Continuity of tangential displacement at the interface with material 1 at $z = h$ gives $W_2(h) = 0$. When this is combined with the requirement that the tangential stress orthogonal to the fibres must vanish at the upper surface, $R_2(2h) = 0$, we obtain the equation

$$q_{21}T_2(h) + q_{22}R_2(h) + q_{23}U_2(h) = 0. \tag{14}$$

Equation (14) allows us to express $R_2(h)$ in terms of $T_2(h)$ and $U_2(h)$ so that $\mathbf{Z}(h)$ and

therefore $\mathbf{Z}(x_1-h)$ for any $h \leqslant x_1 \leqslant 2h$ may be expressed in terms of $\mathbf{X}_2(h) = (T_2(h)U_2(h))^{\mathrm{T}}$. In particular we have that at the upper surface

$$\mathbf{X}_2(2h) = \mathbf{B}\mathbf{X}_2(h) \tag{15}$$

where the components $b_{ij}$ of the $2 \times 2$ matrix $\mathbf{B}$ are given by

$$b_{11} = q_{11} - \frac{q_{12}q_{21}}{q_{22}}, \quad b_{12} = q_{13} - \frac{q_{12}q_{23}}{q_{22}},$$
$$b_{21} = q_{31} - \frac{q_{32}q_{21}}{q_{22}}, \quad b_{22} = q_{33} - \frac{q_{32}q_{23}}{q_{22}}. \tag{16}$$

Adopting the same procedure in the bottom layer of the plate gives the equation

$$\mathbf{X}_2(-2h) = \tilde{\mathbf{B}}\mathbf{X}_2(-h), \tag{17}$$

which may be inverted to give

$$\mathbf{X}_2(-h) = \hat{\mathbf{B}}\mathbf{X}_2(-2h). \tag{18}$$

The matrices $\tilde{\mathbf{B}}$ and $\hat{\mathbf{B}}$ are given in terms of the elements of $\mathbf{B}$ by the expressions

$$\tilde{\mathbf{B}} = \begin{pmatrix} b_{11} & -b_{12} \\ -b_{21} & b_{22} \end{pmatrix}, \quad \hat{\mathbf{B}} = \begin{pmatrix} b_{22} & b_{12} \\ b_{21} & b_{11} \end{pmatrix}, \tag{19}$$

and eqn (18) involves using the result that $\det|\tilde{\mathbf{B}}| = 1$.

The only continuity conditions still to be satisfied at the interfaces $x_1 = \pm h$ give the relations

$$\mathbf{X}_1(-h) = \mathbf{X}_2(-h), \quad \mathbf{X}_2(h) = \mathbf{X}_1(h), \tag{20}$$

and when these are combined with (18), (12) and (15) we obtain

$$\mathbf{X}_2(2h) = \mathbf{M}\mathbf{X}_2(-2h), \tag{21}$$

where

$$\mathbf{M} = \frac{\mathbf{B}\mathbf{R}\hat{\mathbf{R}}\hat{\mathbf{B}}}{\det|\mathbf{R}|}. \tag{22}$$

If the upper surface of the laminate is subject to the impulsive line load

$$t_{11}(x,t) = \rho c_2^2 \delta(x)\delta(t) \tag{23}$$

where $\delta(\cdot)$ is the Dirac delta function, and if the lower surface of the plate is traction free, we have that

$$T_2(2h) = 1, \quad T_2(-2h) = 0. \tag{24}$$

Substituting from (24) into eqn (21) yields

$$U_2(2h) = \frac{m_{22}(k,\hat{s})}{m_{12}(k,\hat{s})}, \quad U_2(-2h) = \frac{1}{m_{12}(k,\hat{s})}, \tag{25}$$

where $m_{ij}$ are the components of the $2 \times 2$ matrix $\mathbf{M}$. Equations (24) and (25) when combined

with (18), (15) and (9) allow us to determine the transforms of normal stress and normal displacement at each of the interfaces. The transforms of the remaining stress and displacement components may then be obtained either at the interfaces or at any interior level in each lamina, using eqns (3), (4), (5), (6), (8) and (14) as required.

Here we shall be particularly concerned with the stresses at the upper and lower surfaces $x_1 = \pm 2h$ at the interfaces $x_1 = \pm h$ and at the mid-plane $x_1 = 0$. At the upper surface $x_1 = 2h$ the normal stress $t_{11}$ is prescribed by eqns (23) and the corresponding transform $T_2(2h)$ is given by (24). The tangential stress $t_{13}$ is zero corresponding to $R_2(2h) = 0$ and the remaining stress transforms are given by eqns (6) in which $T_2$, $W_2$ and $U_2$ are all evaluated at $x_1 = 2h$. The non-zero term for $T_{12}(2h)$ in eqns (6) corresponds to the limiting value on approaching the surface from within the material and this stress component jumps discontinuously to zero at the surface with an associated singularity in the reaction stress $T_{22}(2h)$ in the surface. In eqns (6) the values of $T_2(2h)$ and $U_2(2h)$ are given by (24) and (25) and $W_2(2h)$ may be derived in terms of these in the form

$$W_2(2h) = \frac{q_{43}U_2(2h) - q_{41}T_2(2h)}{q_{44}} = \frac{q_{43}}{q_{44}}\frac{m_{22}(k,s)}{m_{12}(k,s)} - \frac{q_{41}}{q_{44}}, \tag{26}$$

provided $q_{44} \neq 0$. The term $q_{41}/q_{44}$ on the right hand side of eqn (26) makes no contribution to the inverse transforms and may be neglected. The same holds for the term $T_2(2h) = 1$ appearing in some of the expressions in eqn (6) and, in terms of the quantities which contribute to the inverse transforms, the expressions for the stresses at the top surface $x_1 = 2h$ are

$$T_{22}(2h) = -\frac{\rho c_3^2 c_2^2}{c_1^2} 2ikc \frac{q_{43}m_{22}}{q_{44}m_{12}},$$

$$T_{23}(2h) = \rho c_3^2 iks \frac{q_{43}m_{22}}{q_{44}m_{12}}, \quad T_{12}(2h) = \rho c_3^2 iks \frac{m_{22}}{m_{12}},$$

$$T_{33}(2h) = 4\rho c_2^2 ikc\left(1 - \frac{c_2^2}{c_1^2}\right)\frac{q_{43}m_{22}}{q_{44}m_{12}}. \tag{27}$$

At the upper interface, $x_1 = h$, the transforms of normal stress component $T_2(h)$ and normal displacement $U_2(h)$ immediately above the interface are obtained by inverting eqn (15) and using (24) and (25). These yield

$$T_2(h) = b_{22} - \frac{b_{12}m_{22}}{m_{12}},$$

$$U(h) = -b_{21} + \frac{b_{11}m_{22}}{m_{12}}, \tag{28}$$

and continuity at the interface implies that immediately below the interface (in material 1) $T_1(h) = T_2(h)$ and $U_1(h) = U_2(h)$. Continuity of tangential displacements at the interface requires that $W_2(h) = 0$ and $V_1(h) = 0$ and when these are substituted into eqns (6) and (4) respectively we obtain the stress transforms immediately above the interface $T_{ij}^{(2)}$ and immediately below the interface $T_{ij}^{(1)}$ in terms of $T_2 = T_1$ and $U_2 = U_1$. These are

$$T_{22}^{(2)} = -\rho\frac{c_3^2c_2^2}{c_1^2}T_2, \quad T_{33}^{(2)} = \rho\frac{c_2^2}{c_1^2}(c_1^2 - 2c_2^2)T_2,$$

$$T_{23}^{(2)} = 0, \quad T_{31}^{(2)} = -\rho c_2^2\left(\frac{q_{21}T_2 + q_{23}U_2}{q_{22}}\right), \quad T_{12}^{(2)} = \rho c_3^2 iksU_2, \tag{29}$$

and

$$T_{22}^{(1)} = \rho \frac{c_2^2}{c_1^2}(c_1^2 - 2c_2^2)T_1, \quad T_{33}^{(1)} = -\rho \frac{c_2^2 c_2^2}{c_1^2} T_1,$$

$$T_{23}^{(1)} = 0, \quad T_{31}^{(1)} = \rho c_2^2 ikcU_1, \quad T_{12}^{(1)} = \rho c_2^2 \left( \frac{p_{41}T_1 - p_{43}U_1}{p_{42}} \right) \tag{30}$$

where the expression for $T_{31}^{(2)} = \rho c_2^2 R_2(h)$ is obtained from eqn (14) and the expression for $T_{12}^{(1)} = \rho c_2^2 P_1(h)$ is obtained from (7) on using (8). It is clear from these expressions that all the stress components other than $T_{23}$ are discontinuous at the interface.

At the middle surface, $x_1 = 0$, the transforms of normal stress $T_1(0)$ and normal displacement $U_1(0)$ are given by

$$T_1(0) = \left( \frac{r_{22}h_{12} + r_{12}h_{11}}{r_{22}r_{11} - r_{12}r_{21}} \right) \frac{1}{m_{12}}, \quad U_1(0) = \left( \frac{r_{21}h_{12} + r_{11}h_{11}}{r_{22}r_{11} - r_{12}r_{21}} \right) \frac{1}{m_{12}}, \tag{31}$$

and the transforms of tangential stress $P_1(0)$ and tangential displacement $V_1(0)$ are obtained in terms of these from eqns (8), which yield

$$P_1(0) = -\frac{p_{43}}{p_{42}} U_1(0), \quad V_1(0) = -\frac{p_{41}}{p_{44}} T_1(0). \tag{32}$$

The remaining stress transforms at the middle surface are obtained from eqns (4) with $U_1$, $V_1$, $T_1$ given by (31) and (32).

Proceeding in the same way, it is possible to obtain expressions for the stress transforms on either side of the lower interface $x_1 = -h$ and at the bottom surface $x_1 = -2h$.

## 3. INVERSION OF TRANSFORMS

The procedure outlined in the preceding section leads to expressions for the stress and displacement transforms throughout the laminate and it is necessary to invert these transforms in order to recover the dependence on $x$ and $t$. Typical of these in the first of eqns (25) which relates to the normal component of displacement on the upper surface of the plate and for which the inversion integral has the form

$$u_1(2h, x, t) = \frac{1}{4\pi^2 i} \int_{\cdot}^{\cdot} \int_{\eta + i\cdot}^{\eta + i\cdot} \frac{m_{22}(k, \hat{s})}{m_{12}(k, \hat{s})} e^{s't} e^{ikx} \, d\hat{s} \, dk. \tag{33}$$

The integral with respect to $\hat{s}$ may be evaluated in terms of the residues of the integrand at the zeros of the function $m_{12}(k, \hat{s})$ in the left half plane. The equation

$$m_{12}(k, i\omega) = 0 \tag{34}$$

is the dispersion equation for plane wave propagation in the laminate, corresponding to waves travelling in the direction of the normal to the line load under traction free conditions at the two surfaces of the plate. This equation has an infinite number of pairs of roots, $\omega_j = \pm\omega_j(k)$ $(j = 1, 2, \ldots)$, each pair corresponding to forward and backward travelling waves associated with one branch of the dispersion curve. In terms of these solutions, eqn (33) becomes

$$u_1(2h, x, t) = \frac{1}{2\pi} \int_{\cdot}^{\cdot} dk \sum_{j=1}^{\cdot} \left\{ \frac{m_{22}(k, \hat{s})}{dm_{12}/d\hat{s}} e^{ik(x \cdot \cdot t)} \right\}_{\hat{s} = \pm i\omega_j(k)}. \tag{35}$$

Both $m_{12}(k, \hat{s})$ and $m_{22}(k, \hat{s})$ are even functions of $\hat{s}$ and eqn (35) may be written as

$$u_1(2h, x, t) = \frac{i}{\pi} \sum_{j=1}^{\infty} \int_{-\infty}^{\infty} R_j(k) \sin \omega_j(k) t \, e^{ikx} \, dk \tag{36}$$

where

$$R_j(k) = \left[ \frac{m_{22}(k, \hat{s})}{dm_{12}/d\hat{s}} \right]_{\hat{s} = +i\omega_j(k)} = -\left[ \frac{m_{22}(k, \hat{s})}{dm_{12}/d\hat{s}} \right]_{\hat{s} = -i\omega_j(k)}. \tag{37}$$

It may also be shown that $R_j(k)$ is an even function of $k$ and eqn (36) may be further simplified to give

$$u_1(2h, x, t) = \frac{2i}{\pi} \sum_{j=1}^{\infty} \int_{0}^{\infty} R_j(k) \sin \omega_j(k) t \cos kx \, dk. \tag{38}$$

The expression (38) consists of a sum of integrals, one along each branch of the dispersion curve. In general both the integration and summation have to be carried out numerically and we must therefore limit the range of integration to some finite interval $(0, \hat{k})$ and restrict the summation to a finite number of branches $j = 1, \ldots, P$ of the dispersion curve. To carry out the numerical evaluation we choose the values for the material parameters that were previously employed by Green and Baylis (1988) and which relate to a carbon fibre/epoxy resin composite. For the inextensible model, these are $c_1^2/c_2^2 = 4.297$ and $c_3^2/c_2^2 = 2.301$. We have taken as unit of length the thickness $h$ of each ply and as unit of time the quantity $h/c_1$. For a given value of $\gamma$, the dispersion equation has been solved for 18 modes ($P = 18$) with values of $kh$ ranging from zero to 20 ($\hat{k} = 20/h$). Full details of the numerical procedures are to be found in Green and Baylis (1988).

## 4. RESULTS AND DISCUSSION

The nature of transient wave propagation in a plate of isotropic elastic material has been examined in considerable detail by Jones (1964), Weaver and Pao (1982) and by Vasudevan and Mal (1985). The paper by Jones deals with line impact loads which generate an antisymmetric (flexural) motion of the plate and attention is focussed on the bending stress at the upper surface of the plate. The solution is derived in terms of the normal modes of flexural wave propagation, with the stress being expressed as a sum over the modes of a set of infinite integrals with respect to the wavenumber, in a form which is analogous to the expression (38). Jones evaluates these integrals using the stationary phase approximation and gives a comparison between the contributions of each of the first four modes. Weaver and Pao (1982) also adopt the method of normal modes to obtain expressions for the displacements due to any time dependent body force. They examine in detail the normal displacement at the top and bottom surface of the plate produced by a vertical point force imposed on the top surface at time $t = 0$ and held constant for $t > 0$. These authors also discuss the solutions in terms of the stationary phase approximations. In addition they carry out a numerical integration over the first 10 modes, presenting results showing the individual contributions of each of the first five modes as well as giving the overall response due to all 10. The paper by Vasudevan and Mal (1985) deals with the transient surface displacement due to an internal dislocation source and also examines the same surface point load problem as that treated by Weaver and Pao. These authors use transform methods and the propagator matrix technique to obtain the solution. The transform inversion is carried out in a different order from that adopted here, with inversion with respect to wave number $k$ being carried out first to yield the spectral response which is then inverted by Fast Fourier Transform. The separate contributions from individual modes and the overall response obtained by summing over modes show excellent agreement with those of Weaver and Pao.

It is well know that the parameter which governs pulse propagation in dispersive media

is the group velocity $c_g = d\omega/dk$ (see e.g. Achenbach, 1973) and the method of stationary phase brings out the fact that the pulse amplitude decays as $t^{-1/2}$ at large times. A slower rate of decay is associated with the wave fronts, which correspond to the stationary values of the group velocity. These fronts are termed advancing (or mode arrival) when the group velocity is a local maximum and receding (or mode disappearance) when the group velocity has a local minimum. When the stationary value occurs at a finite wavenumber $k$, the form of the disturbance is given by the Airy function and the amplitude decays as $t^{-1/3}$ at large times. When the stationary value for the group velocity is approached asymptotically as $k \to \infty$, the wave front may be associated with a finite or an infinite discontinuity, depending on the behaviour of the integrand for large values of $k$.

We shall shortly present our detailed results for the variation of stresses at various points through the thickness of the laminate. Before doing so, we examine the contributions of individual dispersion curves to the stress response at the top surface of the plate, interpreting these in terms of the associated group velocity. We take as our example the shear stress component $t_{12}$ which jumps discontinuously to a zero across the boundary and for which the limiting value of the transform $T_{12}$ at the upper surface within the material is given in eqn (27) as $\rho c_3^2 sikm_{22}/m_{12}$. Here we discard the factor $\rho c_3^2 s$ and numerically invert the term $ikm_{22}/m_{12}$ to obtain the response $\tau(x, t)$ in the approximate form

$$\tau(x, t) = \sum_{j=1}^{P} \int_0^K k R_j(k) \sin \omega_j(k) t \sin kx \, dk = \sum_{j=1}^{P} \tau_j(x, t), \tag{39}$$

where the residue $R_j(k)$ is defined in eqn (37). All the other stress transforms at the upper surface, given by eqn (27), involve the term $ikq_{43}m_{22}/q_{44}m_{12}$ and since $q_{43}/q_{44}$ is of order one the expression (39) may be taken as representative of the stress state at the top surface of the plate.

The results which we shall shortly present relate to two values of $\gamma$, namely 30° and 60° and in Table 3 we list the quasi-dilatational and quasi-shear wave speeds in both material 1 and material 2 at these angles. These speeds are those associated with the vanishing of $p_1, p_2$ and $q_1, q_2$ and they are given by

$$v_{1d} = (c_1^2 s^2 + c_3^2 c^2)^{1/2}, \quad v_{1s} = (c_2^2 s^2 + c_3^2 c^2)^{1/2},$$
$$v_{2d} = (c_1^2 c^2 + c_3^2 s^2)^{1/2}, \quad v_{2s} = (c_2^2 c^2 + c_3^2 s^2)^{1/2}.$$

Also shown in Table 3 are the surface wave speed at each angle in material 2, $v_{2R}$ and the plate wave speed associated with each angle, $v_B$. This latter is the limiting long wavelength velocity for the fundamental mode of anti-symmetric (flexural) waves in the plate and it is derived in Baylis and Green (1986b). These speeds are given by the expressions

$$v_{2R} = (v_R^2 c^2 + c_3^2 s^2)^{1/2}, \quad v_B = (c_3^2 + c_2^2 s^2)^{1/2}/\sqrt{2}$$

where $v_R$ is the Rayleigh wave velocity for an isotropic material with dilatational wave speed $c_1$ and shear wave speed $c_2$. We have scaled each of these speeds in Table 3 by $c_1$, so that the distance travelled (in units of $h$) may be obtained by multiplying directly by the

Table 3

| $\gamma$ | 30° | 60° |
|---|---|---|
| $v_{1d}$ | 0.807 | 0.940 |
| $v_{1s}$ | 0.678 | 0.555 |
| $v_{2d}$ | 0.940 | 0.807 |
| $v_{2s}$ | 0.555 | 0.678 |
| $v_{2R}$ | 0.535 | 0.673 |
| $v_B$ | 0.545 | 0.596 |

scaled time (measured in units of $h/c_1$). It may be seen from Table 3 that the surface wave speed in the outer material ($v_{2R}$) is less than the quasi-shear wave speed in the inner material ($v_{1s}$) for $\gamma = 30^\circ$ but that for $\gamma = 60^\circ$ the speed $v_{1s}$ is the lowest of all the wave speeds tabulated. We have discussed the consequences of this on the limiting speeds of the dispersion curves in the short wave limit ($kh \to \infty$) in our paper (Green and Baylis, 1988a). There we show that, for the particular numerical values employed here, the short wave limiting speed of both the fundamental symmetric and fundamental anti-symmetric modes is $v_{2R}$, for values of $\gamma < 46.3^\circ$. For all other modes the short wave limiting speed is the lower of $v_{1s}$ and $v_{2s}$, which therefore gives the limit as $v_{2s}$ for $\gamma < 45^\circ$ and $v_{1s}$ for $\gamma > 45^\circ$. We accordingly evaluate the integrals $\tau_j(x, t)$ appearing in eqn (39) for values of $\gamma = 30^\circ$ and $\gamma = 60^\circ$ which provides an example of each of the two possibilities for the limiting behaviour.

In Figs 2–7 we display plots of the dimensionless group velocity, $c_g/c_1$ versus the dimensionless wavenumber $kh$, for a number of modes at both angles of propagation. Also shown in the same figures are the plots of the residue factors $kR_j(k)$ for these modes. All the residue factors are negative and with the exception of Fig. 2 are plotted to the same scale. In order to retain the same range in each figure the factors plotted in Fig. 2 are a half of the actual values. Figures 2 and 3 relate to the fundamental mode of anti-symmetric motion at $\gamma = 30^\circ$ and $\gamma = 60^\circ$ respectively. The two group velocity curves are similar. Each starts in the long wave limit ($kh = 0$) at the appropriate plate speed $v_B$, each rises to a local maximum, falls to a local minimum and finally rises towards an asymptotic value as $kh \to \infty$ (short wave limit). In Fig. 2 this short wave limiting speed is $v_{2R}$ whereas in Fig. 3 the limit is $v_{1s}$. The residue factors in the two figures are strikingly different. Both factors have the same value at $kh = 0$ (the values shown in Fig. 2 must be doubled to obtain the residue factors) but whilst the factor in Fig. 3 drops to zero at the group velocity minimum and remains zero thereafter, that in Fig. 2 continues to increase and approaches a straight line as $kh$ increases. The fundamental modes of symmetric motion differ from these only in the long wavelength limit $kh \to 0$ where, at each angle, the group velocity drops from a maximum and reaches a small negative value at $kh = 0$ and the residue factor at each angle drops to zero at $kh = 0$. Figures 4 and 5 show plots relating to the second anti-symmetric mode at $\gamma = 30^\circ$ and $\gamma = 60^\circ$ respectively. Here the limiting group velocity as $kh \to \infty$ in Fig. 4 is the quasi-shear speed in the outer material, $v_{2s}$, whilst that in Fig. 5 is the quasi-shear speed $v_{1s}$ in the inner material. Once again there is a striking difference between the residue factors in the two figures. The curves shown in Figs 6 and 7 are the group velocity and residue

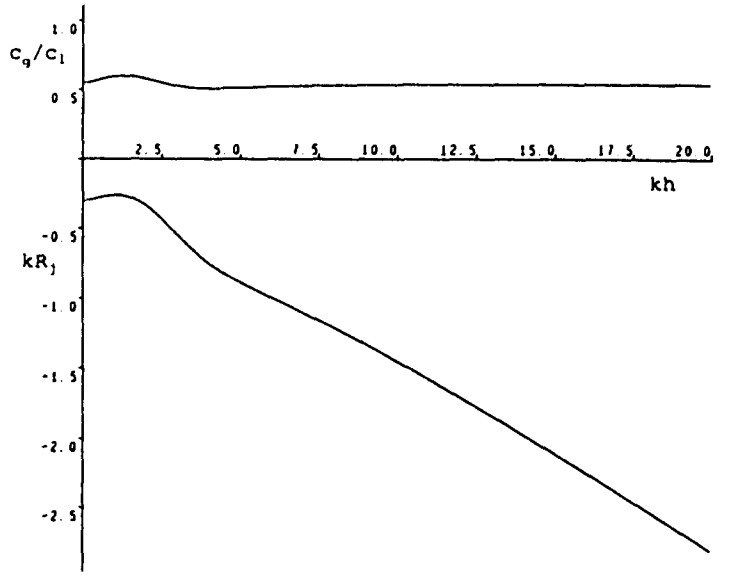


Fig. 2. Group velocity and residue contribution for fundamental mode of anti-symmetric motion at $\gamma = 30^\circ$.

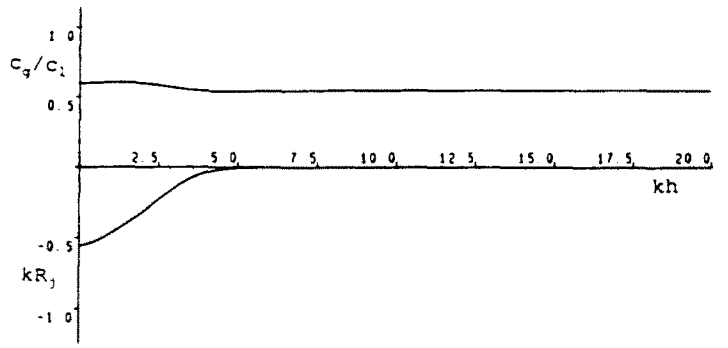


Fig. 3. Group velocity and residue contribution for fundamental mode of anti-symmetric motion at $\gamma = 60°$.

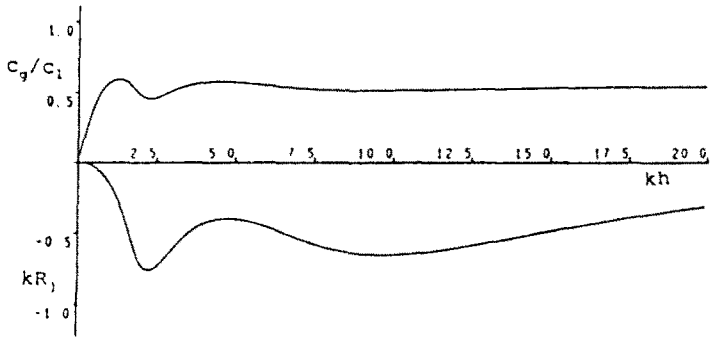


Fig. 4. Group velocity and residue contribution for second mode of anti-symmetric motion at $\gamma = 30°$.

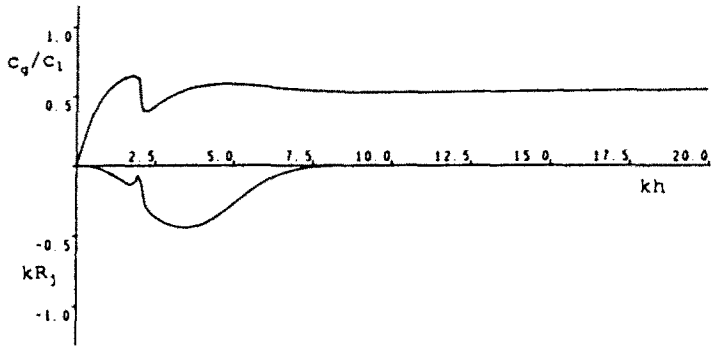


Fig. 5. Group velocity and residue contribution for second mode of anti-symmetric motion at $\gamma = 60°$.

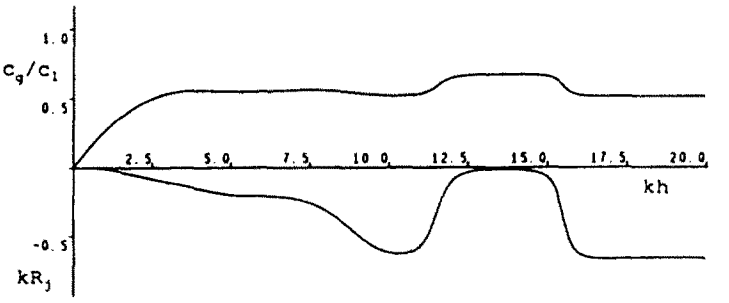


Fig. 6. Group velocity and residue contribution for fifth mode of anti-symmetric motion at $\gamma = 30°$.

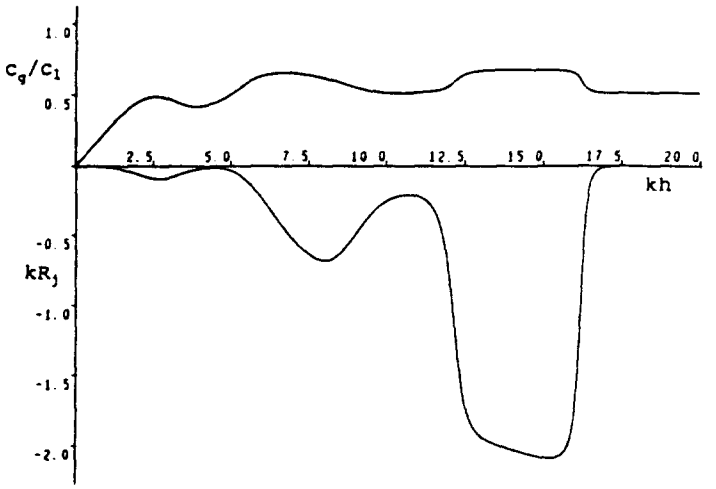


Fig. 7. Group velocity and residue contribution for fifth mode of anti-symmetric motion at $\gamma = 60^\circ$.

factor curves for the fifth anti-symmetric mode at $\gamma = 30^\circ$ and $\gamma = 60^\circ$, respectively. These are chosen as being typical of the curves for the higher harmonics and in both figures the group velocity curves exhibit high and low velocity plateaus on which the speeds are close to the higher and lower of the two quasi-shear speeds $v_{1s}$ and $v_{2s}$. It may be seen from Fig. 6 that at $\gamma = 30^\circ$ the high speed plateau (which corresponds to the inner quasi-shear speed $v_{1s}$) is associated with a small residue factor, whereas the low speed plateau (outer quasi-shear speed $v_{2s}$) is accompanied by a relatively large residue factor. Figure 7 shows a large residue associated with the high speed plateau (which is now the outer quasi-shear speed $v_{2s}$) whilst the residue is small or zero at the low speed ($v_{1s}$).

Figures 8–13 show the individual contributions $\tau_j(x, t)$ to the upper surface shear stress function $\tau(x, t)$ arising from modes 1, 2 and 5 of the anti-symmetric motion at $\gamma = 30^\circ$ and $\gamma = 60^\circ$. Each of these figures shows the variation of the contribution $\tau_j$ as a function of

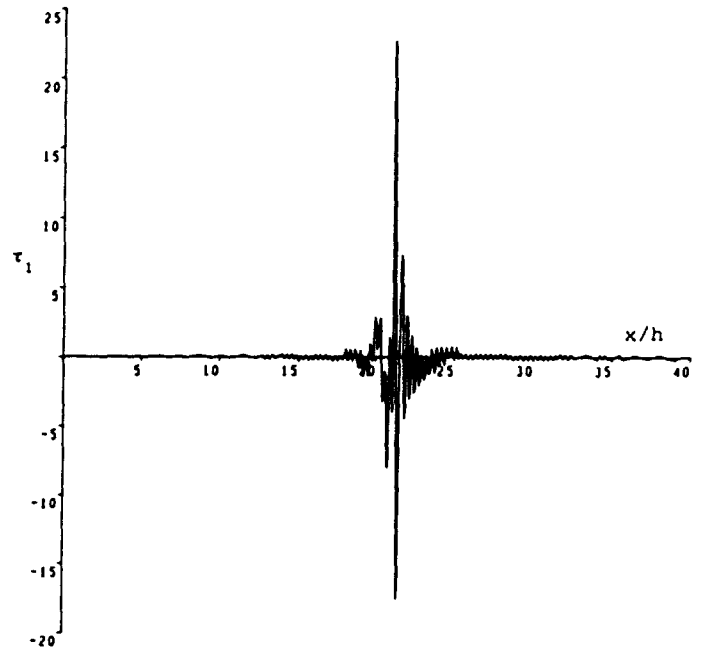


Fig. 8. Stress contribution due to fundamental mode of anti-symmetric motion at $\gamma = 30^\circ$.

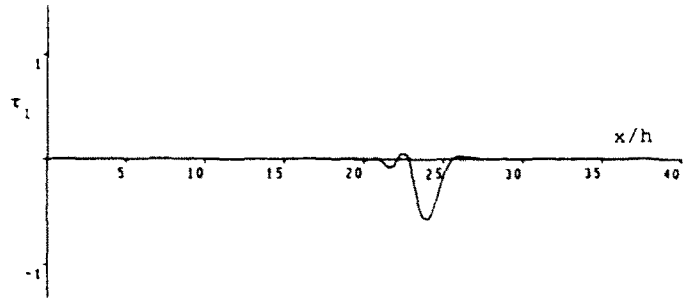


Fig. 9. Stress contribution due to fundamental mode of anti-symmetric motion at $\gamma = 60^\circ$.

$x/h$ at $t = 40h/c_1$. We point out that the plots have differing vertical scales, reflecting the relative contributions from each mode. Figures 8 and 9 relate to $j = 1$ and to the angles $\gamma = 30^\circ$ and $\gamma = 60^\circ$ respectively. Figure 9 shows a small amplitude isolated disturbance travelling with the plate speed $c_B$ whereas the graph in Fig. 8 is completely dominated by the large amplitude high frequency contribution which has travelled a distance $x \approx 21.5h$ corresponding to the speed $c_{2R}$ of the Rayleigh surface wave. Extending the integration range in eqn (39) from $\hat{k}$ to $\infty$ and assuming the residue factor shown in Fig. 2 to continue along the linear portion would lead to a singularity in the stress contribution which travels with the surface wave speed $c_{2R}$. The high frequency oscillation shown in Fig. 8 is a manifestation of the Gibbs' phenomenon, brought about by abruptly terminating the integration at $\hat{k}$ where the residue factor is non-zero. A similar effect is evident to some extent in Figs 10 and 12, which both relate to $\gamma = 30^\circ$ and which correspond to $j = 2$ and $j = 5$, respectively. The corresponding residue factors, shown respectively in Figs 4 and 6, are non-zero at the cut-off limit, $\hat{k} = 20/h$, imposed on the integrals in eqn (39). Figures 9, 11 and 13, which refer to $\gamma = 60^\circ$ and $j = 1$, 2 and 5 respectively, on the other hand, show no trace of this phenomenon and it may be seen from Figs 3, 5 and 7 that in each of these cases the residue factor is zero at $k = \hat{k}$. In evaluating the total response summed over all the modes we have eliminated this high frequency oscillation by use of a windowing function which brings the residues smoothly to zero at the cut-off $\hat{k}$ (see Baylis and Green, 1988 for details).

The stress variation shown in Fig. 11 displays both a forward facing Airy function

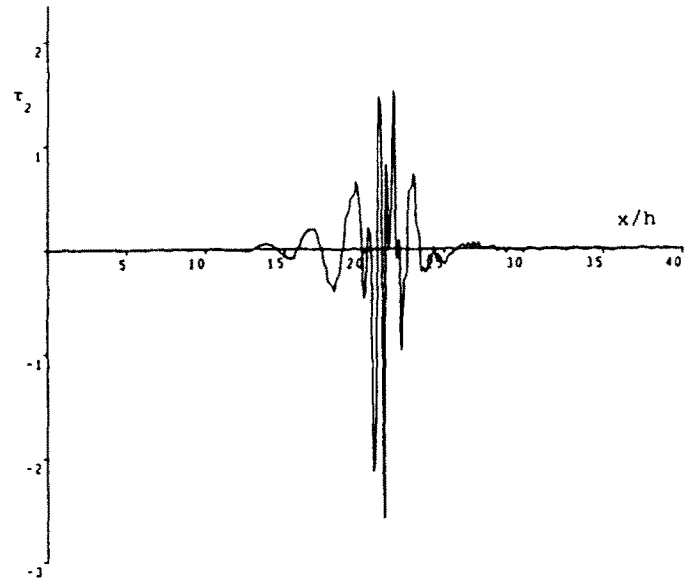


Fig. 10. Stress contribution due to second mode of anti-symmetric motion at $\gamma = 30^\circ$.

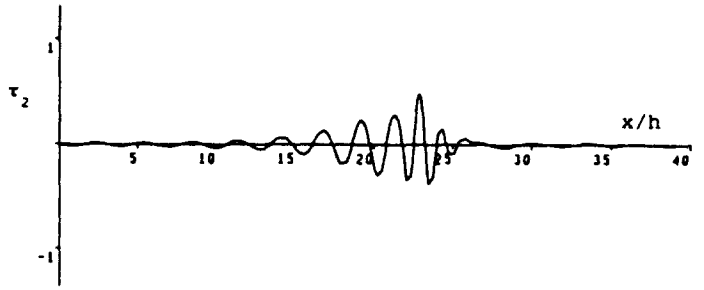


Fig. 11. Stress contribution due to second mode of anti-symmetric motion at $\gamma = 60^\circ$.

oscillation for $x > 24h$ and a backward facing Airy function oscillation for $x < 15h$, which are associated with the local maximum and local minimum values of the group velocity, respectively. Figure 10 also shows a backward facing Airy function for $x < 18h$, associated with the local minimum of the group velocity at $kh \approx 2.25$ but the main feature is again a large amplitude high frequency contribution in the region $20 < x/h < 22$. Of the three modal contributions shown for $\gamma = 60^\circ$ the highest stress amplitude is to be found in Fig. 13 and is associated with the large residue factor shown in Fig. 7 for the high speed plateau region $12.5 < kh < 17.0$. A large residue associated with such a plateau region occurs for values of $kh < 20.0$ in the harmonics $j = 3$ to $j = 6$ and the magnitude of the residue appears to increase linearly with wavenumber. If this behaviour were to persist for $\hat{k} < k < \infty$ then the cumulative effect of all the modes, when integrated over all values of $k$, would give rise to a singularity in the stress travelling at the speed $v_{2s}$ of the quasi-shear wave in the outer layer. The main contribution from the harmonic $j = 5$ at $\gamma = 30^\circ$, shown in Fig. 12, arises from the constant residue factor associated with the low speed plateau which extends from $kh \approx 16$ up to the cut-off point. A constant residue term of this kind is associated with the limiting low velocity plateau of the harmonics $j = 3$ to $j = 6$ in the range up to $kh = 20.0$ and if this persists for $\hat{k} < k < \infty$ then the integrated cumulative effect over all the harmonics would here also give rise to a singular stress travelling with speed $v_{2s}$ of the quasi-shear wave in the outer material. The detailed individual responses shown here only for the anti-symmetric modes are to a large extent reproduced in the symmetric modes. In particular the fundamental symmetric mode has a large surface wave contribution for $\gamma = 30^\circ$ but a very small stress level at $\gamma = 60^\circ$. The upper surface response of the plate is obtained by summing the symmetric and anti-symmetric modes whilst the lower surface response is

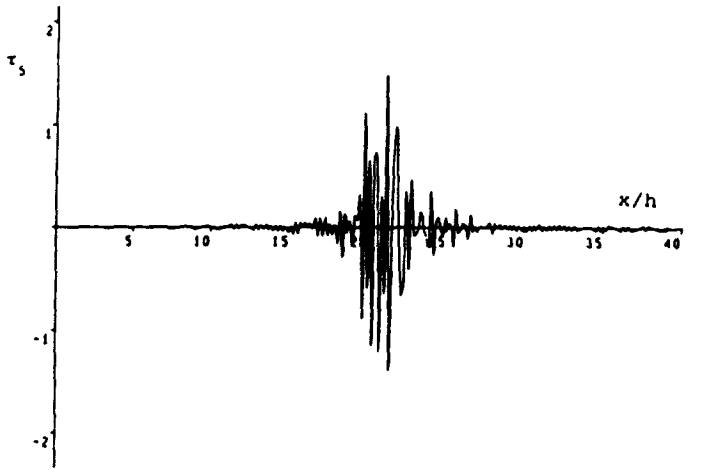


Fig. 12. Stress contribution due to fifth mode of anti-symmetric motion at $\gamma = 30^\circ$.

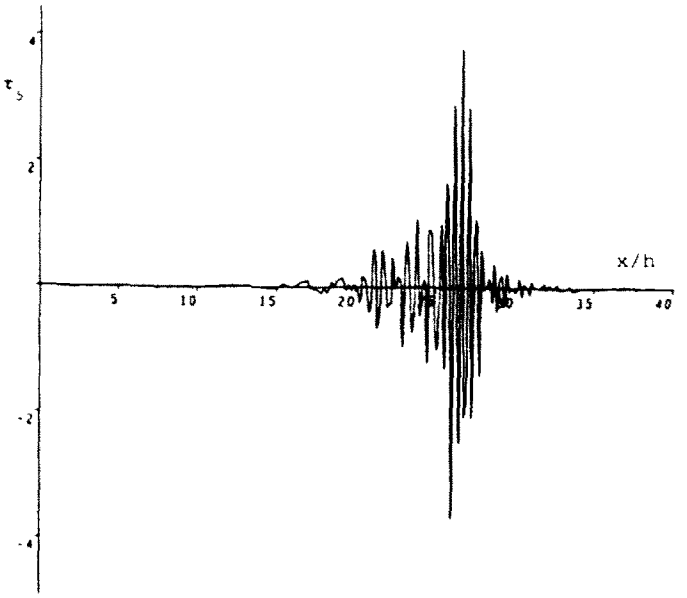


Fig. 13. Stress contribution due to fifth mode of anti-symmetric motion at $\gamma = 60^\circ$.

obtained by subtracting. In consequence the surface wave contributions reinforce each other at the upper surface and cancel out at the lower surface.

We turn now to examine the stress variation through the plate using results obtained by summing over nine anti-symmetric modes and nine symmetric modes. Our first set of curves, Figs 14 and 15, shows the variation of the shear stress component $t_{12}$ as a function of distance $x/h$ from the impact line, at a time of $t = 40h/c_1$ after impact. Each figure consists of five curves showing the stress at the upper surface, the upper interface, the mid-surface, the lower interface and the lower surface, respectively. The non-zero values at the upper and lower surfaces are the discontinuous values parallel to the fibre direction. They are calculated from eqn (27) at the upper surface and its equivalent at the lower surface. The values at the interfaces refer to the outer material in each case and are calculated from eqn (29) at the upper interface and its equivalent at the lower. At each of these interfaces there exist discontinuities in this stress component and the values in the inner material may be determined from eqns (30) but are not displayed here. Finally the mid-surface value is derived from the first of eqns (32) using the expression (31) for $U_1(0)$. Figures 14 and 15 refer to propagation at angles $\gamma = 30^\circ$ and $60^\circ$, respectively. The second set of curves, Figs 16 and 17, has the same format as the first set and again refer to the stress component $t_{12}$, but now at time $t = 200h/c_1$ after impact. The most obvious feature of thee two sets of curves is the large stress amplitude to be seen on the upper surface for propagation at angle $30^\circ$ (Figs 14 and 16). The distance of this disturbance from the impact point shows in each case that it is associated with the Rayleigh surface wave which propagates at this angle but which does not exist at $\gamma = 60^\circ$ (Figs 15 and 17). Another significant feature to be seen in all the curves is the low level of shear stress at the mid-surface as compared with the level in the outer material at the interfaces and at the upper and lower surfaces. This high shear stress load in the outer layers is consistent with the shearing behaviour of inextensible materials under bending loads (see Rogers and Pipkin, 1971) since the shear stress component $t_{12}$ is associated with the inextensibility direction in the outer layers. In all these figures there is some disturbance evident at distances associated with the faster of the two quasi-shear speeds at each angle. For $\gamma = 30^\circ$ this fastest wave speed is that in the inner material ($c_{1s}$) and the associated stress level is small, with the main pulse travelling at a speed close to that of the quasi-shear wave in the outer material ($c_{2s}$). For $\gamma = 60^\circ$ it is the speed $c_{2s}$ in the outer material which is the greater and there is in this case a significant

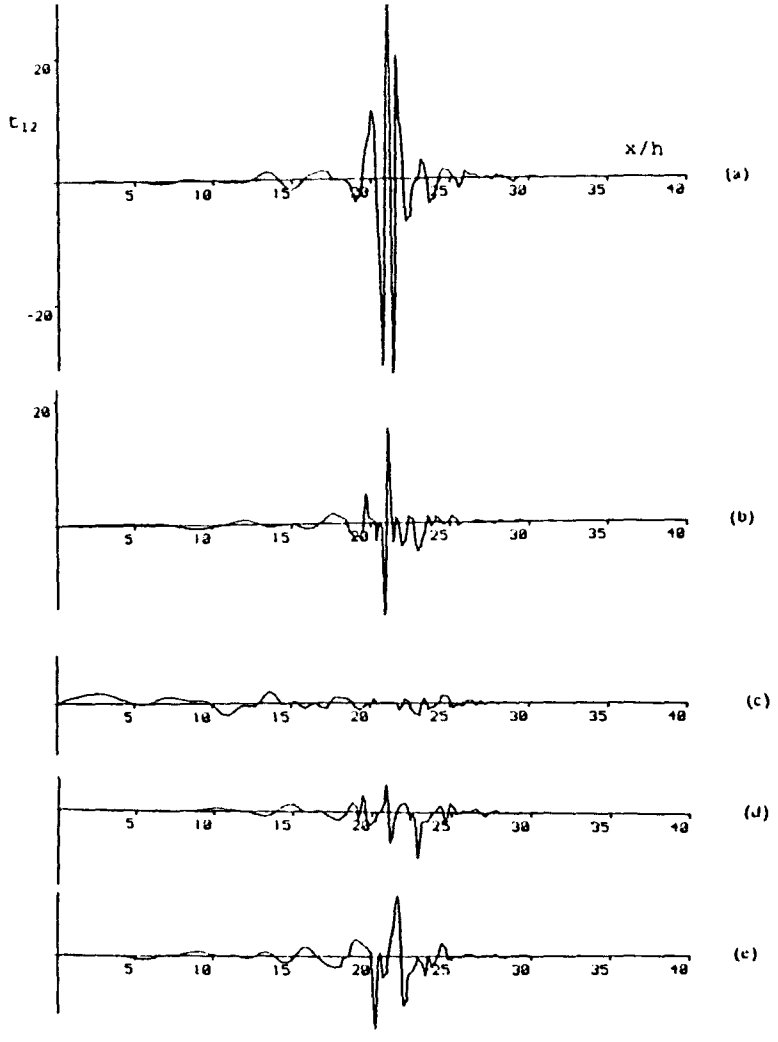


Fig. 14. Stress component $t_{12}$ at time $t = 40h/c_1$ for $\gamma = 30^\circ$ at : (a) upper surface, (b) upper interface, (c) mid-surface, (d) lower interface, (e) lower surface.

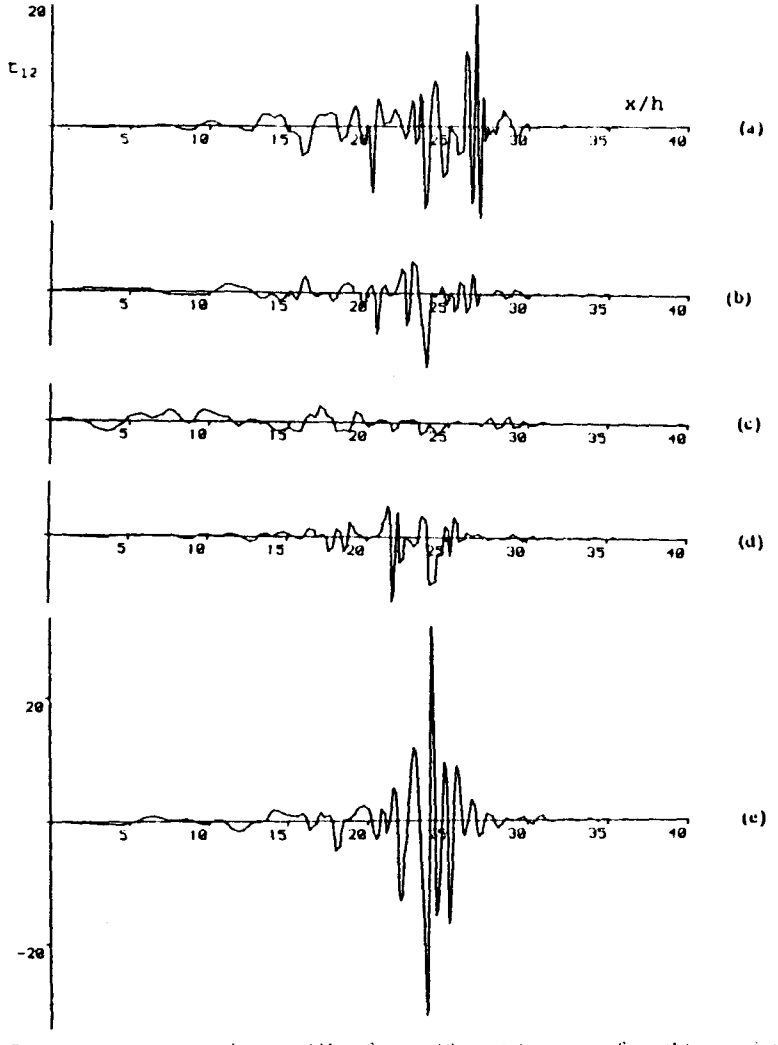


Fig. 15. Stress component $t_{12}$ at time $t = 40h/c_1$ for $\gamma = 60^\circ$ at : (a) upper surface, (b) upper interface, (c) mid-surface, (d) lower interface, (e) lower surface.

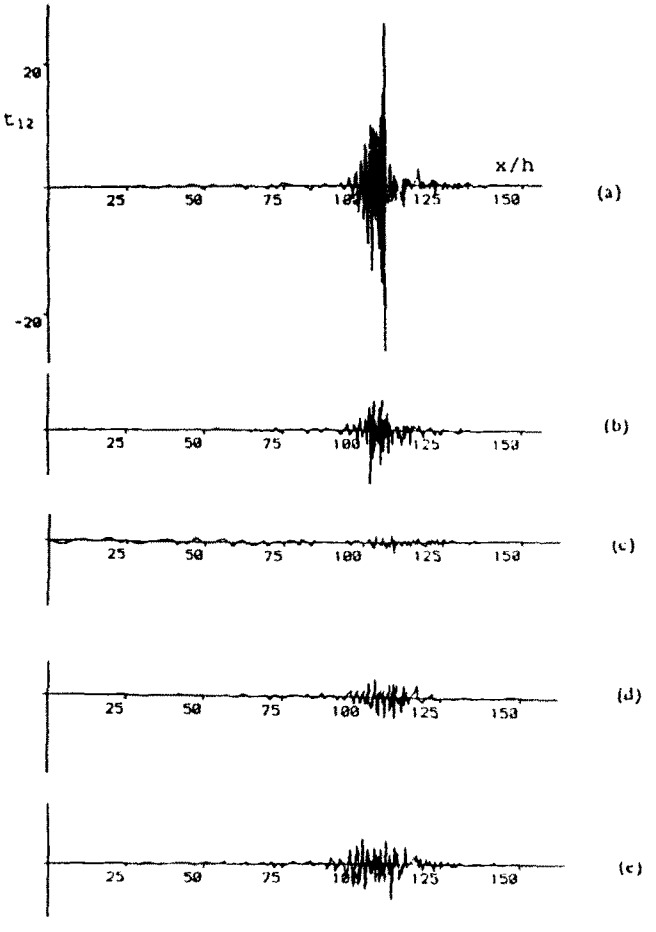


Fig. 16. Stress component $t_{12}$ at time $t = 200h/c_1$ for $\gamma = 30^\circ$ at: (a) upper surface, (b) upper interface, (c) mid-surface, (d) lower interface, (e) lower surface.

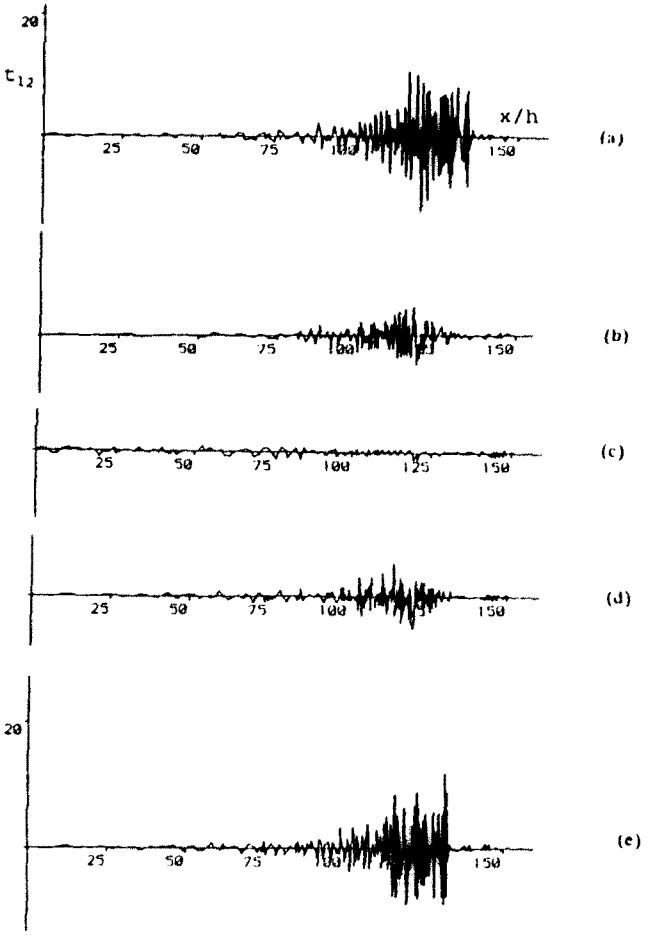


Fig. 17. Stress component $t_{12}$ at time $t = 200h/c_1$ for $\gamma = 60^\circ$ at: (a) upper surface, (b) upper interface, (c) mid-surface, (d) lower interface, (e) lower surface.

stress level associated with this speed which gives a pulse extending over a much longer distance than that for $\gamma = 30^\circ$.

The next two sets of curves (Figs 18 and 19 and Figs 20 and 21) show the variation of the shear stress component $t_{13}$ with distance from the impact line at times $t = 40h/c_1$ (Figs 18 and 19) and $t = 200h/c_1$ (Figs 20 and 21). These again relate to angles of propagation $\gamma = 30^\circ$ (Figs 18 and 20) and $\gamma = 60^\circ$ (Figs 19 and 21). The three curves displayed in each figure give the stress at the upper interface, at the mid-surface and at the lower interface respectively. At the upper surface and the lower surface, the shear stress component $t_{13}$ is zero. In each of these figures, the interface stress is calculated in the outer material (material 2), using the expression in eqns (29) at the upper interface and its equivalent at the lower interface. There is a discontinuity in this stress component across the upper and lower interface and the value in the inner material at the upper interface may be determined using eqns (30), but this is not displayed here. We note, however, from eqns (29) and (30) that the stress component $t_{13}^{(1)}$ in the inner material [eqns (30)] is obtained from the stress component $t_{12}^{(2)}$ at the interface in the outer material [eqns (29)] by multiplying by the factor $\cot\gamma$ so that the qualitative behaviour of the stress $t_{13}^{(1)}$ may be deduced from Figs 14–17.

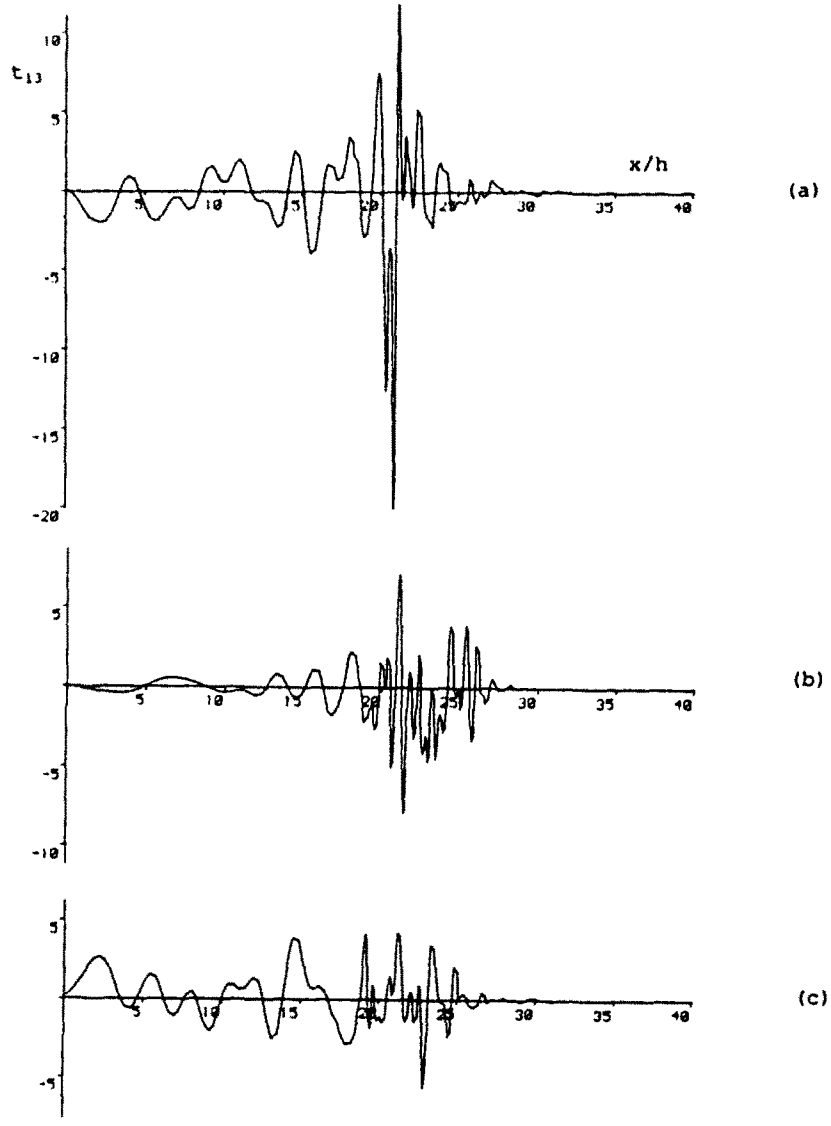


Fig. 18. Stress component $t_{13}$ at time $t = 40h/c_1$ for $\gamma = 30^\circ$ at: (a) upper surface, (b) mid-surface, (c) lower interface.

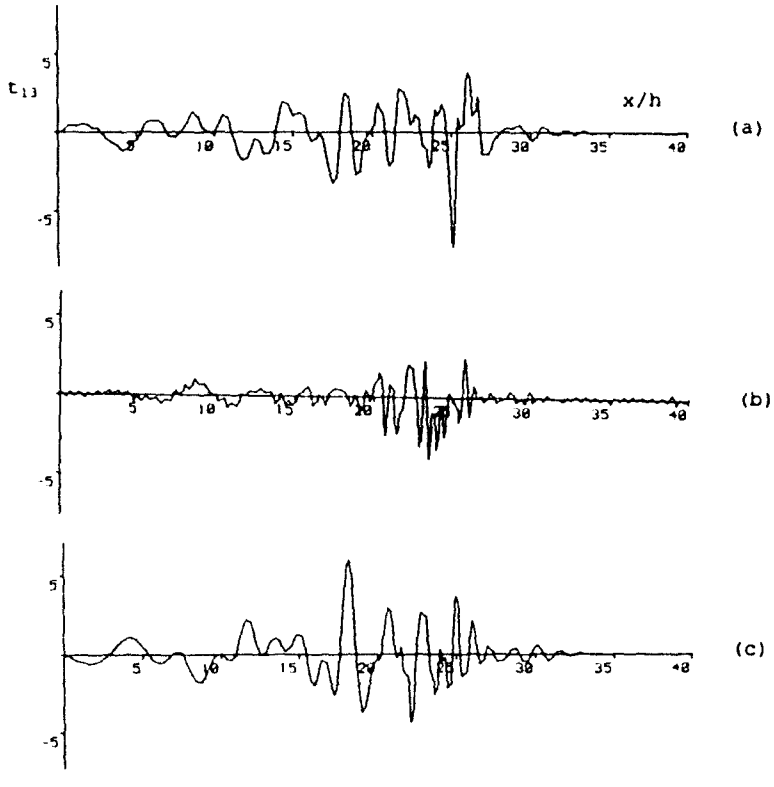


Fig. 19. Stress component $t_{13}$ at time $t = 30h/c_1$ for $\gamma = 60^\circ$ at: (a) upper surface, (b) mid-surface, (c) lower interface.

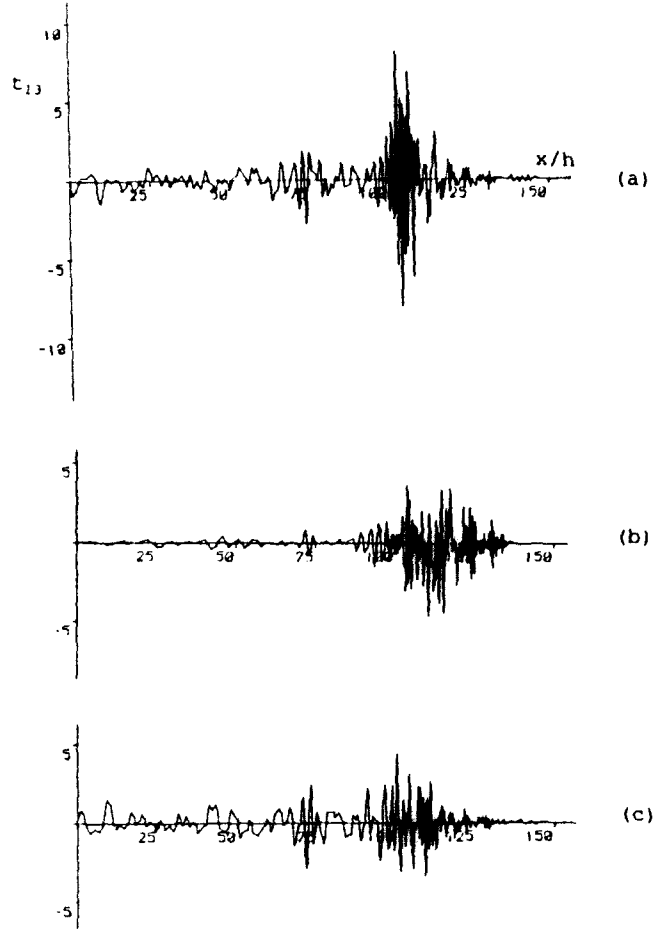


Fig. 20. Stress component $t_{13}$ at time $t = 200h/c_1$ for $\gamma = 30^\circ$ at: (a) upper surface, (b) mid-surface, (c) lower interface.

In discussing the sets of curves displayed in Figs 18–21, we recall that the stress component $t_{13}$ refers to the shear stress parallel to the fibre direction in the inner material. Figures 18 and 20 which relate to the angle 30° clearly show that the effect of the Rayleigh surface wave is transmitted down through the upper layer to the first interface but that this effect dies out within the inner material and is not apparent at the mid-surface nor at the lower interface. At angle 60° (Figs 19 and 21), the stress level throughout the inner core material is low, showing that there is little shearing along the fibre direction.

The sets of curves in Figs 22–25 relate to the in-plane stress component $t_{22}$. Again, Figs 22 and 23 are at time $t$ for which $t = 40h/c_1$ and Figs 24 and 25 correspond to $t = 200h/c_1$. Each figure consists of four curves which give $t_{22}$ at the upper surface [eqn (27)], at the upper interface in the outer material [eqns (29)], at the lower interface in the outer material and at the bottom surface. It may be seen from eqns (27) and (29) that the stress component $t_{33}$ at the outer surfaces and at the two interfaces in the outer material are obtained from $t_{22}$ on multiplication by a factor. Furthermore, eqns (30) show that in the inner material at the interfaces the stress component $t_{33}$ is equal to the component $t_{22}$ at the same interface in the outer material. These stress components all refer to the continuous stress value within the respective materials but there also exist singular stresses along the fibres at each interface and at the outer surfaces. Thus there are singularities in $t_{22}^{(2)}$ for the outer material at $x_1 = \pm 2h$ and $x_1 = \pm h$ with singularities in $t_{33}^{(2)}$ in the inner material at $x_1 = \pm h$.

The curves shown in this set of figures correspond to propagation at angle 30° (Figs 22 and 24), and 60° (Figs 23 and 25). The main feature here also is the stress level associated with the Rayleigh surface wave at 30° which does not exist at 60°. Another significant feature, evident in all the figures but particularly so in Figs 24 and 25, is the presence of a slow moving low frequency disturbance at the interface which is not present at the outer surfaces.

Finally, in Figs 26 and 27 we present a comparison between the shear stress levels $t_{13}$

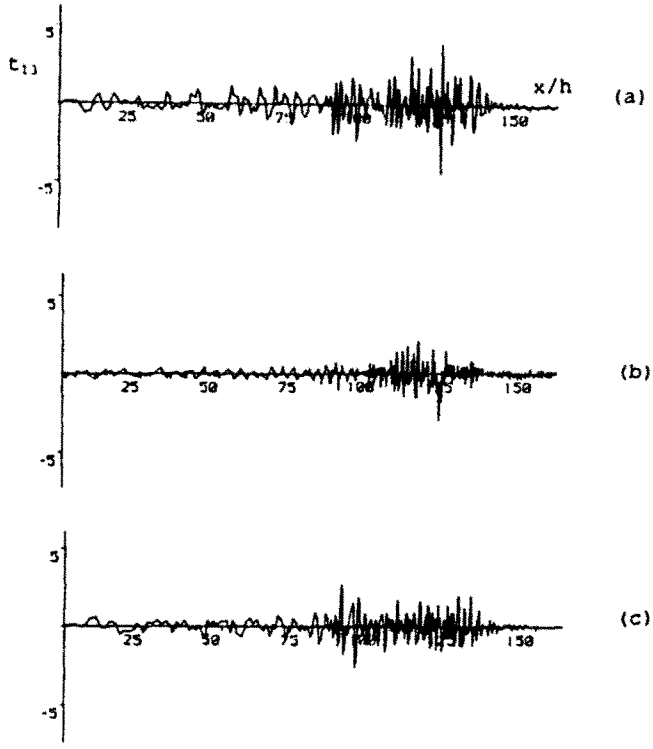


Fig. 21. Stress component $t_{13}$ at time $t = 200h/c_1$ for $\gamma = 60°$ at: (a) upper surface, (b) mid-surface, (c) lower interface.

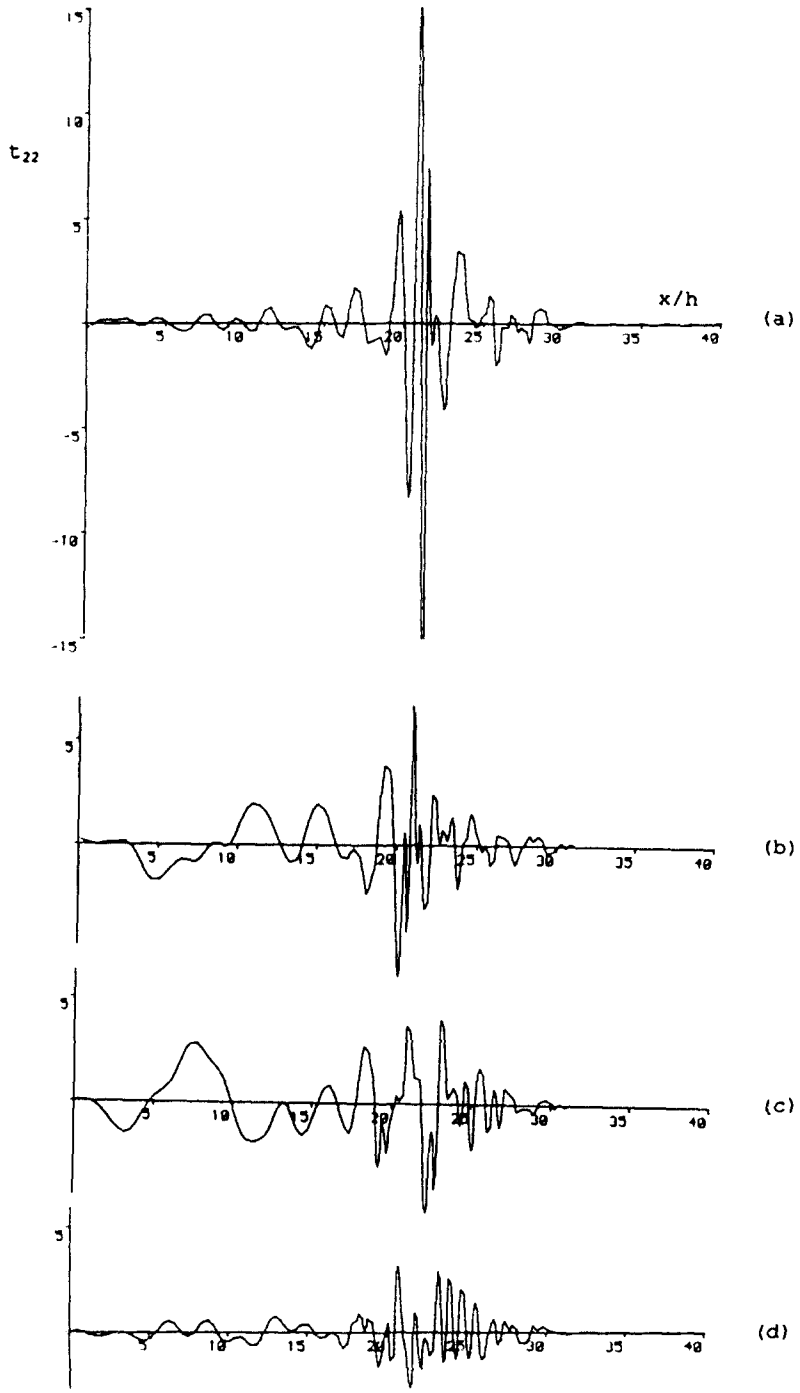


Fig. 22. Stress component $t_{22}$ at time $t = 40h/c_1$ for $\gamma = 30$ at : (a) upper surface, (b) upper interface, (c) lower interface, (d) lower surface.

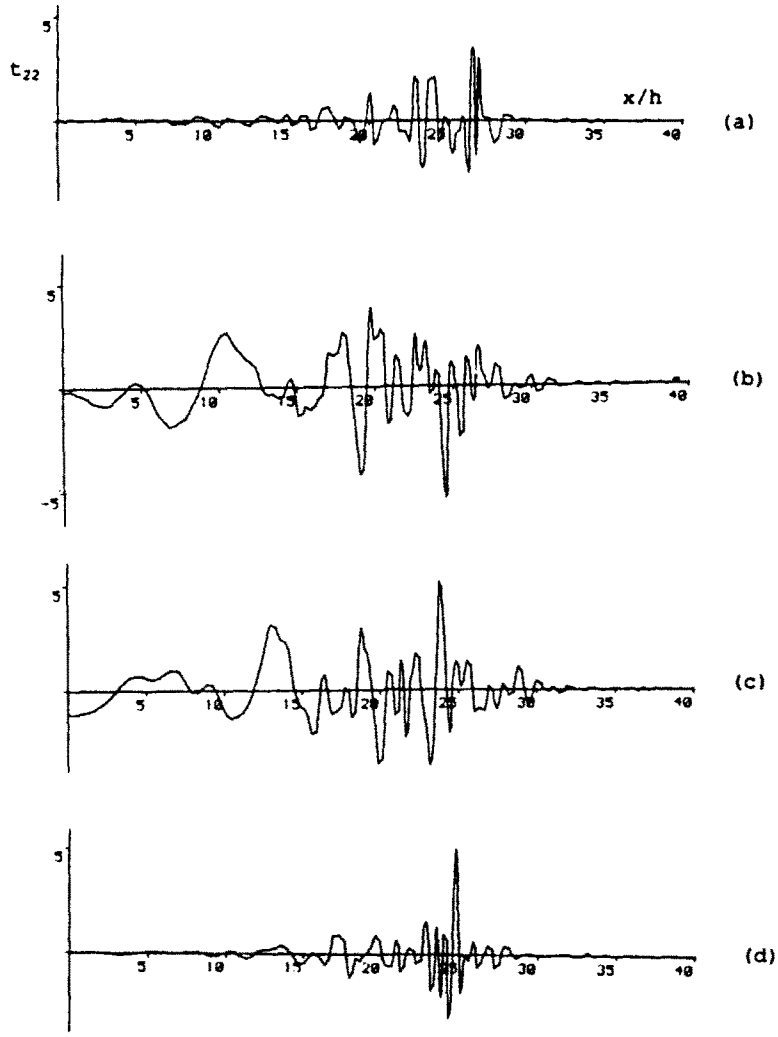


Fig. 23. Stress component $t_{22}$ at time $t = 40h/c_1$ for $\gamma = 60^\circ$ at : (a) upper surface, (b) upper interface, (c) lower interface, (d) lower surface.

in the inextensible material (Fig. 26) and in the extensible material (Fig. 27). These figures relate to the fundamental mode of anti-symmetric motion for propagation along the fibre direction ($\gamma = 0^\circ$). Each figure consists of five curves, associated with five different values of the wavenumber ($kh$), which correspond to wavelengths ranging from approximately $7.0h$ to approximately $0.8h$. All the curves show the variation of the shear stress component $t_{13}$ through one half of the plate as a function of scaled distance $x_1/h$ from the mid-surface. The numerical values $t_{13}$ are, in each case, scaled by the value of the bending stress component at the same wavelength calculated at the outer surface, $t_{33}^*$. With the exception of curves (a), the corresponding curves in each figure show a remarkable similarity except for the narrow band in the region of the interface ($x_1/h \approx 1.0$), where the inextensible material exhibits the discontinuity and the extensible material shows a rapid variation of shear stress in order to maintain continuity. Curve (a) in Fig. 26 shows a very high level of shear stress in the core material as compared with that of curve (a) in Fig. 27. This is a reflection of the fact that, in the long wavelength limit, the inextensible material is incapable of sustaining the St. Venant bending mode associated with a linear variation of normal stress $t_{33}$ through the thickness but deforms rather through shearing (Rogers and Pipkin, 1971). Further detailed comparisons of stress levels are to be found in Baylis (1986).

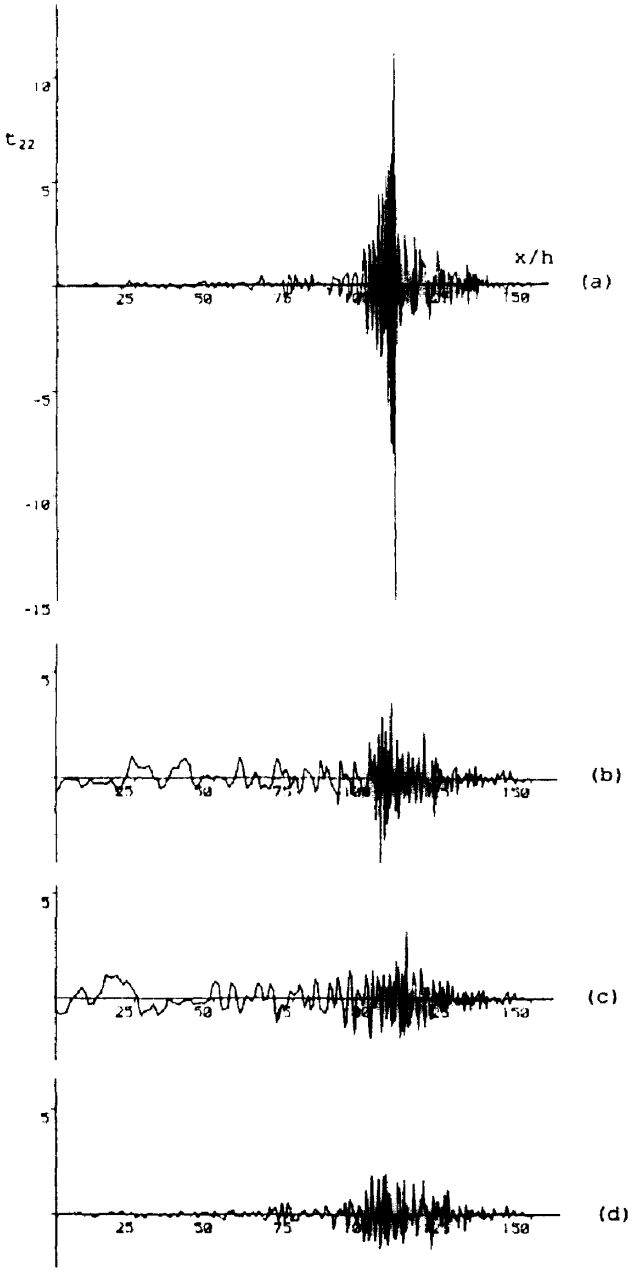


Fig. 24. Stress component $t_{22}$ at time $t = 200h\,c_1$ for $\gamma = 30^\circ$ at: (a) upper surface, (b) upper interface, (c) lower interface, (d) lower surface.

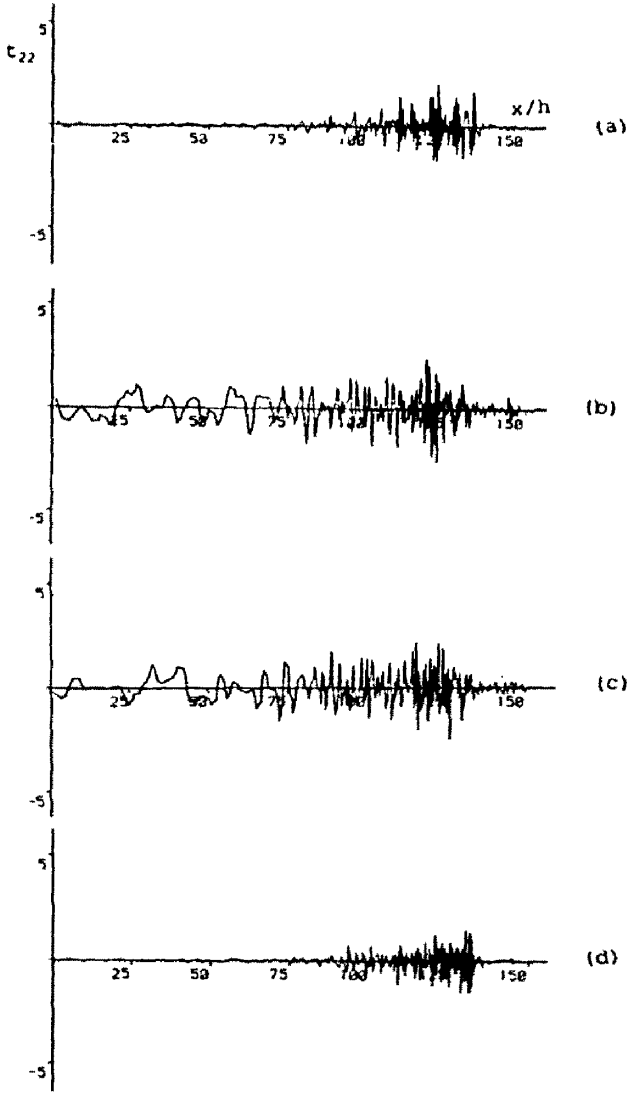


Fig. 25. Stress component $t_{22}$ at time $t = 200h/c_1$ for $\gamma = 60^\circ$ at: (a) upper surface, (b) upper interface, (c) lower interface, (d) lower surface.

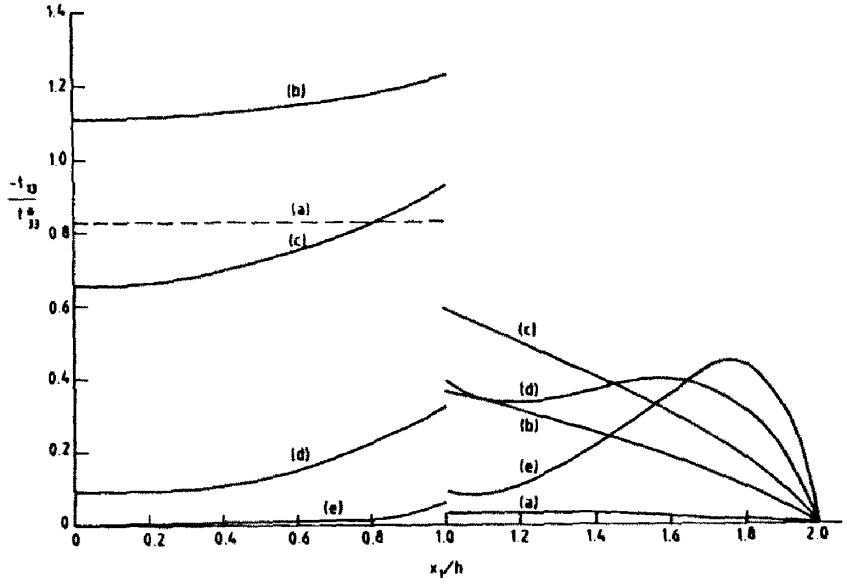


Fig. 26. Variation of shear stress $t_{13}$ through a four-ply plate of inextensible material. (a) $kh = 0.091$, (b) $kh = 0.945$, (c) $kh = 1.836$, (d) $kh = 3.685$, (e) $kh = 7.552$. [The values shown by the dashed line for case (a) must be multiplied by a factor 10 to get the correct stress level.]

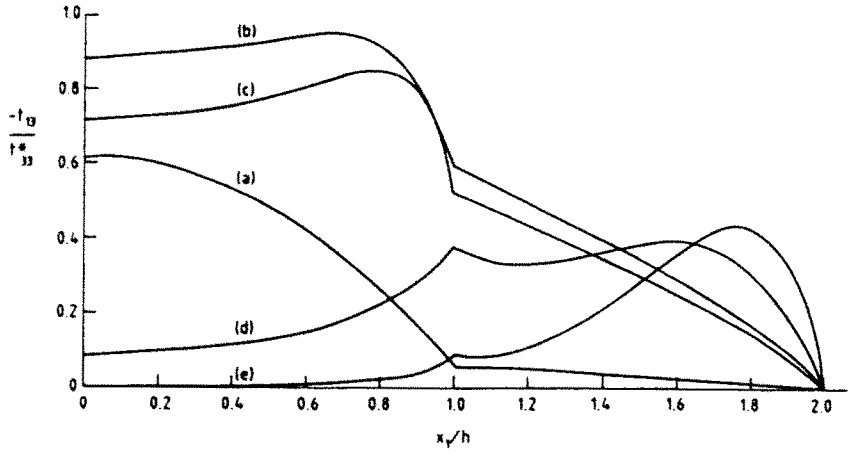


Fig. 27. Variation of shear stress $t_{13}$ through a four-ply plate not subject to the inextensibility constraint. (a) $kh = 0.075$, (b) $kh = 1.374$, (c) $kh = 1.729$, (d) $kh = 3.669$, (e) $kh = 7.530$.

*Acknowledgement*—This work is supported by the U.S. Air Force Office of Scientific Research under grant number AFOSR-88-0353.

## REFERENCES

Achenbach, J. D. (1973). *Wave Propagation in Elastic Solids*. North Holland, Amsterdam.
Baylis, E. R. (1986). Wave propagation in fibre-reinforced laminates. Ph.D. Thesis, University of Nottingham.
Baylis, E. R. and Green, W. A. (1986a). Flexural waves in fibre-reinforced laminated plates, *J. Sound Vib.* **110**, 1–26.
Baylis, E. R. and Green, W. A. (1986b). Flexural waves in fibre-reinforced laminated plates, Part II. *J. Sound Vib.* **111**, 181–190.
Baylis, E. R. and Green, W. A. (1988). Impact stress waves in fibre-reinforced laminated plates. *Proc. 3rd Int. Conf. on Recent Advances in Structural Dynamics*, AFWAL-TR-88-3034, Vol. 1, pp. 171–183.
Ceranoglu, A. N. and Pao, Y. H. (1981). Propagation of elastic pulses and acoustic emission in a plate. *ASME J. Appl. Mech.* **48**, 125–147.
Chow, T. S. (1971). On the propagation of flexural waves on an orthotropic laminated plate and its response to an impulse load. *J. Composite Mater.* **5**, 306–319.
Green, W. A. (1982). Bending waves in strongly anisotropic elastic plates. *Q. J. Mech. Appl. Math.* **35**, 485–507.
Green, W. A. and Baylis, E. R. (1988a). The contribution of high-harmonics to transient waves in plates and laminates. *Proc. 3rd Int. Conf. on Recent Advances in Structural Dynamics*, AFWAL-TR-88-3034, Vol. 1, pp. 185–197.
Green, W. A. and Baylis, E. R. (1988b). The propagation of impact stress waves in anisotropic fibre reinforced laminates. In *Wave Propagation in Structural Composites* (Edited by T. C. T. Ting and A. K. Mal), Vol. 90, pp. 53–67. ASME, New York.
Green, W. A. and Milosavljević, D. (1985). Extensional waves in strongly anisotropic elastic plates. *Int. J. Solids Structures* **21**, 343–353.
Jones R. P. N. (1964). Transverse impact waves in a bar under conditions of plane-strain elasticity. *Q. J. Mech. Appl. Math.* **17**, 401–421.
Kreis, A. and Sayir, M. (1983). Propagation of flexural waves in a thin transversely isotropic plate. *ZAMP* **34**, 816–831.
Lee, J. D., Du, S. and Liebowitz, H. (1984). Three-dimensional finite element and dynamic analysis of composite laminate subject to impact. *Comput. Struct.* **19**, 807–813.
Mal, A. K. (1988). Wave propagation in layered composite laminates under periodic surface loads. *Wave Motion* **10**, 257–266.
Miklowitz, J. (1978). *The Theory of Elastic Waves and Waveguides*. North Holland, Amsterdam.
Moon, F. C. (1972). Wave surface due to impact on anisotropic plates. *J. Composite Mater.* **6**, 62–79.
Rogers, T. G. and Pipkin, A. C. (1971). Plane deformations of incompressible fibre-reinforced materials. *J. Appl. Mech.* **38**, 1047–1061.
Sun, C. T. (1973). Propagation of shock waves in anisotropic composite plates. *J. Composite Mater.* **7**, 366–382.
Vasudevan, N. and Mal, A. K. (1985). Response of an elastic plate to localized transient sources. *ASME J. Appl. Mech.* **52**, 356–362.
Weaver, R. L. and Pao, Y. H. (1982). Axisymmetric elastic waves excited by a point source in a plate. *ASME J. Appl. Mech.* **49**, 821–836.
Willis, J. R. and Bedding, R. J. (1978). Transient elastodynamic fields in anisotropic plates and layers. In *Modern Problems in Elastic Wave Propagation* (Edited by J. Miklowitz and J. D. Achenbach). John Wiley, New York.
Wu, H. T. and Springer, G. S. (1988). Impact induced stresses and delaminations in composite plates. *J. Composite Mater.* **22**, 533–560.